JCTC Journal of Chemical Theory and Computation

Article

Cite This: J. Chem. Theory Comput. 2019, 15, 2517−2534

pubs.acs.org/JCTC

Low-Temperature Quantum Fokker−Planck and Smoluchowski Equations and Their Extension to Multistate Systems

Tatsushi Ikeda* and Yoshitaka Tanimura*

Department of Chemistry, Graduate School of Science, Kyoto University, Kyoto 606-8502, Japan

Supporting Information

ABSTRACT: Simulating electron−nucleus coupled dynamics poses a nontrivial challenge and an important problem in the investigation of ultrafast processes involving coupled electronic and vibrational dynamics. Because irreversibility of the system dynamics results from thermal activation and dissipation caused by the environment, in dynamical studies, it is necessary to include heat bath degrees of freedom in the total system. When the system dynamics involves high-energy electronic transitions, the environment is regarded to be in a low-temperature regime and we must treat it quantum mechanically. In this Article, we present rigorous and versatile approaches for investigating the dynamics of open systems with coupled electronic and vibrational degrees of freedom within a fully quantum mechanical framework. These approaches are based on a quantum Fokker−Planck equation and a quantum Smoluchowski equation employing a heat bath with an Ohmic spectral density, with non-Markovian low-temperature correction terms, and extensions of these equations to the case of multistate systems. The accuracy of these equations was numerically examined for a single-state Brownian system, while their applicability was examined for multistate double-well systems by comparing their results with those of the fewest-switch surface hopping and Ehrenfest methods with a classical Markovian Langevin force. Comparison of the transient absorption spectra obtained using these methods clearly reveals the importance of the quantum low-temperature correction terms. These equations allow us to treat nonadiabatic dynamics in an efficient way, while maintaining numerical accuracy. The C++ source codes that we developed, which allow for the treatment of the phase and coordinate space dynamics with any single-state or multistate potential forms, are provided as Supporting Information.

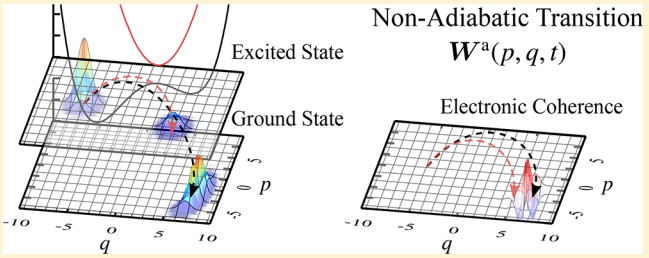

1. INTRODUCTION

Understanding nonadiabatic dynamics in electronic and bionanomaterials is fundamentally important in the study of many types of phenomena, ranging from photoisomerization to spintronics. Recent advances in experimental technologies have made it possible to observe such nonadiabatic processes that take place on very short time scales.[1−5] Theoretical input regarding the complex profiles of potential energy surfaces (PESs) and the nonadiabatic coupling among PESs is important for analyzing such ultrafast transport processes, in particular, those in materials involving biomolecular aggregates and crystalline solar cells.[6,7] For such systems, the surrounding molecules act as a heat bath and also play an essential role in determining the nature of the transport processes because they either promote or suppress the wavepacket motion of the system through thermal activation and relaxation.

In the study of systems of the type considered here, while nuclear motion is often treated using a semiclassical approach, which is applicable to the case of heavy nuclei, nonadiabatic transition processes must be described using a purely quantum mechanical approach because transitions between discretized electronic states are, in their essence, quantum dynamics. For this reason, the effect of the environment should be treated using an open quantum model, even if the dynamics of the nuclei are semiclassical, because otherwise the quantum nature of the electronic transitions is not properly accounted for. Indeed, ignoring the quantum effects of the environment, in particular in the low temperature regime, in which quantum effects become very important, leads to unphysical behavior. For example, in the case that we employ a classical description of the environment in the low temperature regime, while electronic transitions and the motion of wavepackets are described by quantum mechanics, the positivity of the probability distributions of the electronic states cannot be maintained. This is a fundamental complication, known as the "positivity problem," which imposes a well-known limitation on the applicability of the quantum master equation without the rotating wave approximation.[8,9] The positivity problem arises because the classical treatment of the environment leads to the violation of the quantum fluctuation−dissipation (QFD) theorem.[10−13]

The excited state dynamics of systems exhibiting ultrafast coupled electronic and vibrational dynamical processes have been investigated with models that explicitly take into account nuclear degrees of freedom and electronic states through

Received: November 28, 2018
Published: February 18, 2019

DOI: 10.1021/acs.jctc.8b01195
J. Chem. Theory Comput. 2019, 15, 2517−2534

approaches employing equations of motion for wave functions, density matrices, phase space distributions,[14−22] and Gaussian quantum wavepackets[23−25] and approaches utilizing mixed quantum-classical trajectories.[26−28] However, many of these approaches were developed for isolated systems and were verified within the system which have a few degrees of freedom. Moreover, varieties of assumptions (in particular, assumptions regarding the quantum dynamical treatment of the couplings between the electronic states and the nuclear coordinates) were introduced in such approaches and the assumptions severely limit their range of applicability. In contrast, the multistate quantum hierarchical Fokker−Planck equation (MS-QHFPE) approach, which is an extension of the quantum Fokker−Planck equation for the Wigner distribution function[29−32] to multistate systems[16−20] and is a variant of the hierarchical equations of motion (HEOM) theories,[13,33,34] can treat any types of diabatic coupling and PES profiles with non-Markovian system−bath interactions described by a Drude spectral density. However, although the MS-QHFPE approach allows us to compute the dynamics described by a multistate system−bath Hamiltonian numerically rigorously, integrating the equations of motion is very computationally intensive, in particular, for a system described by multidimensional PESs. Hence, presently, calculations carried out for two-dimensional systems are limited to the high-temperature Markovian case described by the MS-QFPE.[20]

While it has been found that non-Markovian effects arising from non-Ohmic environments are important in the description of exciton/electron transfer phenomena,[6,7,35,36] the Ohmic heat bath model for nuclear dynamics has been (implicitly) employed in many investigations for models described by PESs that further coupled to a heat-bath, including a model that causes a Brownian/Drude spectral density after reducing the nuclear degrees of freedom.[37−40] This results from the fact that the non-Markovian effects on the nuclear motion so far studied are regarded to be insignificant in such systems, in particular, when the damping on the nuclear motion is quite strong. For this reason, although there have been several investigations employing Drude environments for the nuclear dynamics carried out on systems including nonlinear vibrational responses,[41−43] a ratchet system,[44] and a resonant tunneling diode system,[45,46] in this Article, we derive equations of motion for single-state and multistate systems employing the Ohmic environment: low-temperature quantum Fokker−Planck equations (LT-QFPE) and low-temperature quantum Smoluchowski equations (LT-QSE) and their extensions to multistate (MS) systems, MS-LT-QFPE and MS-LT-QSE. As seen in the theory of quantum Brownian motion, within a quantum mechanical description, an Ohmic bath exhibits peculiar behavior in momentum space.[47−49] We show that this difficulty can be avoided by properly treating the low temperature correction terms in the LT-QFPE and MS-LT-QFPE. In the case of a heat bath with an Ohmic spectral density, the LT-QFPE and LT-QSE are sufficiently accurate, while also being sufficiently simple in comparison to the QHFPE. These features make the LT-QFPE and LT-QSE suited for describing slowly decaying systems and systems rendered in multidimensional phase spaces. Also, it is noteworthy that many of the existing formalisms, including those of the quantum Fokker−Planck equation[29−32] and Zusman equation,[50−52] can be derived from the (MS-)LT-QFPE and (MS-)LT-QSE under certain conditions.

The organization of this paper is as follows. In section 2, we introduce a model with multiple electronic states described by the PESs that are coupled to a harmonic heat bath with an Ohmic spectral density. Then, we present the MS-LT-QFPE and MS-LT-QSE and their single PES forms, LT-QFPE and LT-QSE. In section 3, we present numerical results for single-state Brownian and multistate double-well systems to illustrate the validity and applicability of these approaches. Section 4 is devoted to concluding remarks. The C++ source codes that we developed are provided as Supporting Information.

2. HAMILTONIAN AND FORMALISM

2.1. Model. Because the LT-QFPE and LT-QSE are the simpler, single-potential forms of the MS-LT-QFPE and MS-LT-QSE, we start with a multipotential system. We consider a molecular system with multiple electronic states $\{|j\rangle\}$ coupled to the nuclear coordinates. For simplicity, we represent the nuclear coordinates by a single dimensionless coordinate, q. Here and hereafter, we employ a dimensionless coordinate and a dimensionless momentum defined in terms of the actual coordinate and momentum, $\overline{q}$ and $\overline{p}$, as $q \equiv \overline{q}\sqrt{m\omega_0/\hbar}$ and $p \equiv \overline{p}/\sqrt{m\hbar\omega_0}$, where ω_0 is the characteristic vibrational frequency of the system and m is the effective mass. The reaction coordinate is also bilinearly coupled to the harmonic bath coordinates, $\vec{x} \equiv (..., x_\xi, ...)$. The Hamiltonian of the total system is expressed as[29]

$$\hat{H}_{\mathrm{tot}}(p, q; \vec{p}, \vec{x}) \equiv \hat{H}(p, q) + \hat{H}_{\mathrm{B}}(\vec{p}, \vec{x}; q) \tag{1}$$

where the system Hamiltonian, $\hat{H}(p, q)$, is defined as

$$\hat{H}(p, q) \equiv \frac{\hbar\omega_0}{2}\hat{p}^2 + \sum_{j,k} |j\rangle U^{\mathrm{d}}_{jk}(\hat{q})\langle k| \tag{2}$$

Here, the nuclear and electronic operators are denoted by hats, and the direct products with the unit operator in the kinetic and bath terms ($\otimes\hat{1}$) are omitted. The diagonal element $U^{\mathrm{d}}_{jj}(q)$ is the diabatic PES of $|j\rangle$, and the off-diagonal element $U^{\mathrm{d}}_{jk}(q)$ ($j \neq k$) represents the diabatic coupling between $|j\rangle$ and $|k\rangle$. The vibrational frequency $\overline{\omega}$ at a local minimum of the potential q_0 is determined by the curvature of the PESs as

$$\hbar\overline{\omega} \simeq \sqrt{\hbar\omega_0 \frac{\partial^2}{\partial q^2} U_{j_0 j_0}(q)\Big|_{q=q_0}} \tag{3}$$

where j_0 is a primary state of the vibrational dynamics. Therefore, the frequency ω_0 is chosen to be $\hbar\omega_0 \simeq \partial^2 U_{j_0 j_0}(q)/\partial q^2|_{q=q_0}$ to have $\overline{\omega} \simeq \omega_0$. The bath Hamiltonian $\hat{H}_{\mathrm{B}}(\vec{p},\vec{x};q)$ is defined as

$$\hat{H}_{\mathrm{B}}(\vec{p}, \vec{x}; q) \equiv \sum_\xi \frac{\hbar\omega_\xi}{2}\left[\hat{p}_\xi^{\,2} + \left(\hat{x}_\xi - \frac{g_\xi}{\omega_\xi}\hat{q}\right)^2\right] \tag{4}$$

where ω_ξ, p_ξ, and g_ξ are the vibrational frequency, conjugate momentum, and system-bath coupling constant of the ξth dimensionless bath mode, x_ξ. The bath is characterized by the dissipation and fluctuation that it engenders. These are represented by the relaxation function

$$R(t) = \frac{2}{\pi}\int_0^\infty d\omega \frac{\mathcal{J}(\omega)}{\omega}\cos\omega t \tag{5a}$$

DOI: 10.1021/acs.jctc.8b01195
J. Chem. Theory Comput. 2019, 15, 2517−2534

and the symmetrized correlation function

$$C(t) = \frac{2}{\pi}\int_0^\infty d\omega \mathcal{J}(\omega)\left(n(\omega) + \frac{1}{2}\right)\cos\omega t \tag{5b}$$

where the spectral density is defined as $\mathcal{J}(\omega) \equiv \pi\Sigma_\xi(g_\xi^2/2)\delta(\omega - \omega)$, and we have introduced the Bose−Einstein distribution function, $n(\omega) \equiv (e^{\beta\hbar\omega} - 1)^{-1}$, for the inverse temperature divided by the Boltzmann constant, $\beta \equiv 1/k_B T$.

We choose the coefficients ν_k and η_k so as to realize the relation

$$n(\omega) + \frac{1}{2} \simeq \frac{1}{\beta\hbar}\frac{1}{\omega} + \sum_k^K \frac{2\eta_k}{\beta\hbar}\frac{\omega}{\omega^2 + \nu_k^2} \tag{6}$$

for finite K, where the first term on the right-hand side is the classical contribution from the temperature, and the remaining terms are the quantum low-temperature (QLT) corrections. The Matsubara decomposition scheme (MSD) can be applied straightforwardly to the above. In this scheme, we set $\eta_k = 1$ and $\nu_k = \tilde{\nu}_k$, where $\tilde{\nu}_k \equiv 2\pi k/\beta\hbar$ is the kth Matsubara frequency.[34,53] In this Article, we employ the Padé spectral decomposition $[N-1/N]$ (PSD$[N-1/N]$) scheme to enhance the computational efficiency while maintaining the accuracy.[54−56]

To reduce the computational times for the computations of the nonadiabatic dynamics with any forms of the PESs, here we employ an Ohmic spectral density, expressed as

$$\mathcal{J}(\omega) = \frac{\zeta}{\omega_0}\omega \tag{7}$$

where ζ is the system-bath coupling strength. Then we have

$$R(t) = \frac{\zeta}{\omega_0}\cdot 2\delta(t) \tag{8a}$$

and

$$C(t) \simeq C_K(t) = \frac{\zeta}{\omega_0}\left(\frac{1}{\beta\hbar} + \sum_k^K \frac{2\eta_k}{\beta\hbar}\right)\cdot 2\delta(t) - \sum_k^K \frac{\zeta}{\omega_0}\frac{2\eta_k}{\beta\hbar}\cdot\nu_k e^{-\nu_k|t|} \tag{8b}$$

In the case of a harmonic PES with frequency ω_0, the conditions $\zeta < 2\omega_0$, $\zeta = 2\omega_0$, and $\zeta > 2\omega_0$ correspond to the underdamped, critically damped, and overdamped cases, respectively. In Figure 1, we plot $C_K(t)$ for various values of the cutoff K, at the temperature $\beta\hbar\omega_0 = 7.47$. As this figure and eq 8b indicate, the fluctuation term is always non-Markovian because of the quantum nature of the noise, and it can be regarded as Markovian only in the high-temperature limit, $\beta\hbar\omega_0 \ll 1$, in which the heat bath exhibits classical behavior.[13,57] This is an important conclusion obtained from the QFD theorem, namely, that the negative non-Markovian terms appear in the case that we do not use a time-coarse-grained, Markovian description. Note that, in the case that we employ an ohmic spectral density without cutoff functions (e.g., Lorentzian cutoff and exponential cutoff), some of the physical observables, including the mean square of the momentum, $\langle p^2\rangle$, diverge due to the divergence of the first and second terms in eq 8b under the infinite summation of the Matsubara frequencies, if there is no finite cutoff function. This divergence is often referred to as the ultraviolet divergence.[47−49] In practice, we can ignore QLT correction terms whose frequencies are sufficiently greater than the characteristic frequency of the system, because the random force generated by such terms is averaged out over a sufficiently short time scale that its influence on the dynamics of interest is negligible. In this way, we are able to calculate nondiverging physical observables, for example, the mean square of the coordinate, $\langle q^2\rangle$, by simply ignoring the contribution from the high-frequency QLT correction terms by implementing the cutoff K, while diverging physical observables still tend to diverge.

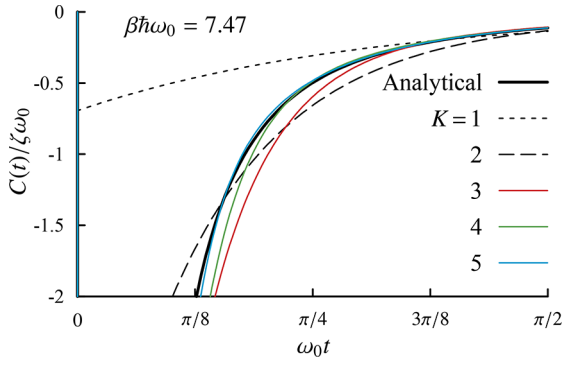

Figure 1. Symmetrized correlation function, $C(t)$, for an Ohmic spectral density, eq 7, at temperature $\beta\hbar\omega_0 = 7.47$, which is in the low-temperature regime. The thick black solid curve represents the exact expression, eq 5b, and the other curves represent $C_K(t)$, eq 8b, for various values of the cutoff, K. The values of the coefficients ν_k and η_k for each value of K are given in Table 1. The fast decay components in the exact expression and the delta-function components in eq 8b, which are overlapped with the $t = 0$ axis, are not displayed.

Table 1. PSD[N-1/N] Coefficients Used for K = 1−5

K	k	$\beta\hbar\nu_k$	η_k
1	1	7.745967	2.5
2	1	6.305939	1.032824
	2	19.499618	5.967176
3	1	6.2832903	1.000227
	2	12.9582867	1.300914
	3	36.1192894	11.198859
4	1	6.283185	1.000000
	2	12.579950	1.015314
	3	20.562598	1.905605
	4	57.787940	18.079081
5	1	6.283185	1.000000
	2	12.566542	1.000262
	3	19.004690	1.113033
	4	29.579276	2.800147
	5	84.536926	26.586558

2.2. Multistate Low-Temperature Quantum Fokker−Planck Equations. The state of the total system is represented by the density operator, $\hat{\rho}_{tot}(z,z',\vec{x},\vec{x}') \equiv \langle\vec{x}|\langle z|\hat{\rho}_{tot}(t)|z'\rangle|\vec{x}'\rangle$, where $|z\rangle$ and $|\vec{x}\rangle$ are the eigenstate of the system and bath coordinate operators, respectively. We consider the reduced density matrix in the diabatic representation of the system subspace, defined as

$$\rho_{jk}^{d}(z, z', t) \equiv \langle j|\hat{\rho}(z, z', t)|k\rangle \tag{9}$$

where $\hat{\rho}(z,z', t) \equiv Tr_B\{\hat{\rho}_{tot}(z, z', \vec{x}, \vec{x}', t)\}$ is the reduced density operator and $Tr_B\{...\} \equiv \int d\vec{x} \int d\vec{x}'\delta(\vec{x}-\vec{x}')\{...\}$ represents the trace operation in the bath subspace. The

DOI: 10.1021/acs.jctc.8b01195
J. Chem. Theory Comput. 2019, 15, 2517−2534

diagonal and off-diagonal elements, ρ_{jj}^{d} and ρ_{jk}^{d} $(j \neq k)$, represent the population of $|j\rangle$ and the coherence between $|j\rangle$ and $|k\rangle$, respectively. Hereafter, we employ the matrix forms of the reduced density matrix and the diabatic PESs: $\{\boldsymbol{\rho}^{\mathrm{d}}(z, z')\}_{jk} \equiv \rho_{jk}^{\mathrm{d}}(z,z')$ and $\{\boldsymbol{U}^{\mathrm{d}}(z)\}_{jk} \equiv U_{jk}^{\mathrm{d}}(z)$.

We now introduce the Wigner distribution function, which is the quantum analogy of the classical distribution function in phase space. For a multistate system, the multistate Wigner distribution function (MS-WDF) is defined as[16−20]

$$\boldsymbol{W}^{\mathrm{d}}(p, q, t) \equiv \frac{1}{2\pi}\int \mathrm{d}r e^{-ipr}\boldsymbol{\rho}^{\mathrm{d}}\left(q + \frac{r}{2}, q - \frac{r}{2}\right) \tag{10}$$

where $q \equiv (z + z')/2$ and $r \equiv z - z'$. Both p and q are now c-numbers in this phase space representation.

The reduced dynamics of $\boldsymbol{\rho}^{\mathrm{d}}(z, z', t)$ and $\boldsymbol{W}^{\mathrm{d}}(p, q, t)$ are expressed in the path integral framework using the Feynman−Vernon influence functional.[58] Their time evolutions can be described by a set of time differential equations in the HEOM form (see section S1). In the present case, these equations are

$$\begin{aligned}
&\frac{\partial}{\partial t}\boldsymbol{W}_{\vec{n}}^{\mathrm{d}}(p, q, t)\\
&= -\left(\mathcal{L}_{\mathrm{qm}}^{\mathrm{d}}(p, q) + \sum_k^K n_k\nu_k + \hat{\Xi}_K^{\mathrm{d}}(p, q)\right)\boldsymbol{W}_{\vec{n}}^{\mathrm{d}}(p, q, t)\\
&\quad - \sum_k^K \hat{\Phi}^{\mathrm{d}}(p, q)\boldsymbol{W}_{\vec{n}+\vec{e}_k}^{\mathrm{d}}(p, q, t)\\
&\quad - \sum_k^K n_k\nu_k\hat{\Theta}_k^{\mathrm{d}}(p, q)\boldsymbol{W}_{\vec{n}-\vec{e}_k}^{\mathrm{d}}(p, q, t)
\end{aligned} \tag{11}$$

where $\vec{n} \equiv (..., n_k, ...)$ is a K-dimensional multi-index whose components are all non-negative integers and $\vec{e}_k \equiv (0, ..., 1, 0, ...)$ is the kth unit vector. The multi-index $\vec{n}$ represents the index of the hierarchy, and physically, the first hierarchical element, $\boldsymbol{W}_0^{\mathrm{d}}(p, q, t)$, corresponds to the MS-WDF, $\boldsymbol{W}^{\mathrm{d}}(p, q, t)$. The rest of the hierarchical elements serve only to facilitate treatment of the non-Markovian system-bath interaction that arises from the QLT effects.

The quantum Liouvillian for the MS-WDF is given by

$$\mathcal{L}_{\mathrm{qm}}^{\mathrm{d}}(p, q) \equiv \mathcal{K}(p, q) + \mathcal{U}_{\mathrm{qm}}^{\mathrm{d}}(p, q) \tag{12a}$$

where

$$\mathcal{K}(p, q)\boldsymbol{W}(p, q) \equiv \omega_0 p\frac{\partial}{\partial q}\boldsymbol{W}(p, q) \tag{12b}$$

and

$$\begin{aligned}
&\mathcal{U}_{\mathrm{qm}}^{\mathrm{d}}(p, q)\boldsymbol{W}(p, q)\\
&\quad \equiv \frac{i}{\hbar}(\boldsymbol{U}^{\mathrm{d}}(q)\bigstar\boldsymbol{W}(p, q) - \boldsymbol{W}(p, q)\bigstar\boldsymbol{U}^{\mathrm{d}}(q))
\end{aligned} \tag{12c}$$

are the kinetic and potential terms in the diabatic representation, respectively. Here, we have introduced the star operator, ★, which represents the Moyal product, defined as[59,60]

$$\bigstar \equiv \exp\left[\frac{i}{2}\left(\overleftarrow{\partial}_q\overrightarrow{\partial}_p - \overrightarrow{\partial}_q\overleftarrow{\partial}_p\right)\right] \tag{13}$$

The differentiation operators from the left and right appearing here are defined as

$$\overrightarrow{\partial}_x f(x) = f(x)\overleftarrow{\partial}_x \equiv \frac{\partial f(x)}{\partial x} \tag{14}$$

The operators for the fluctuation and dissipation, $\hat{\Phi}^{\mathrm{d}}(p, q)$, $\hat{\Theta}_k^{\mathrm{d}}(p, q)$, and $\hat{\Xi}_k^{\mathrm{d}}(p, q)$, appearing in eq 11, are defined as

$$\hat{\Phi}^{\mathrm{d}}(p, q) \equiv -\frac{\partial}{\partial p} \tag{15a}$$

$$\hat{\Theta}_k^{\mathrm{d}}(p, q) \equiv \frac{\zeta}{\omega_0}\frac{2\eta_k}{\beta\hbar}\frac{\partial}{\partial p} \tag{15b}$$

and

$$\begin{aligned}
\hat{\Xi}_K^{\mathrm{d}}(p, q) \equiv &-\frac{\zeta}{\omega_0}\frac{\partial}{\partial p}\left(\omega_0 p + \frac{1}{\beta\hbar}\frac{\partial}{\partial p}\right)\\
&+ \sum_k^K \hat{\Phi}^{\mathrm{d}}(p, q)\hat{\Theta}_k^{\mathrm{d}}(p, q)
\end{aligned} \tag{15c}$$

The first two operators in the above equations, $\hat{\Phi}^{\mathrm{d}}(p, q)$ and $\hat{\Theta}_k^{\mathrm{d}}(p, q)$, arises from eq 8a and the first term in eq 8b, while the last operator, $\hat{\Xi}_K^{\mathrm{d}}(p, q)$, arises from the second term in eq 8b. The derivation of eq 11 is presented in section S1.B. Because eq 11 is a generalization of the multistate quantum Fokker−Planck equation (MS-QFPE)[16−19] valid in the low-temperature regime, we refer to these equations as the multistate low-temperature quantum Fokker−Planck equations (MS-LT-QFPE).

For a single-state system, the matrices $\boldsymbol{W}^{\mathrm{d}}(p, q, t)$ and $\boldsymbol{U}^{\mathrm{d}}(q)$ reduce to scalar functions, $W(p, q, t)$ and $U(q)$. In this case, we refer to eq 11 as the low-temperature quantum Fokker−Planck equations (LT-QFPE). These equations can be understood as an extension of the quantum Fokker−Planck equation (QFPE).[29−32]

The conventional (multistate) quantum hierarchical Fokker−Planck equations ((MS-)QHFPE) with a Drude spectral density, $\mathcal{J}^{\mathrm{D}}(\omega) \propto \omega{\gamma_{\mathrm{D}}}^2/(\omega^2 + {\gamma_{\mathrm{D}}}^2)$, where γ_{D} is the cutoff frequency, are capable of treating systems subject to non-Markovian noise, and are not limited to the case of an Ohmic spectral density.[32,42,44,46] However, the (MS-)QHFPE require a $(K + 1)$-dimensional multi-index $\vec{n}' \equiv (n_0, \vec{n})$ (i.e., the additional index n_0) to describe non-Markovian dynamics caused by a finite value of γ_{D} and, therefore, is computationally more expensive than the (MS-)LT-QFPE. Moreover, the (MS-)QHFPE become unstable in the ohmic limit (i.e., $\gamma_{\mathrm{D}} \gg 1$) at low temperatures because of the fast decaying terms with γ_{D}, while the (MS-)LT-QFPE is sufficiently accurate and also being sufficiently simple in comparison to the (MS-)QHFPE. Thus, although applicability of these equations is limited to the ohmic case, the computational cost to solve the (MS-)LT-QFPE is suppressed than that to solve the (MS-)QHFPE. These features make the (MS-)LT-QFPE and (MS-)LT-QSE suited for describing slowly decaying systems and systems rendered in multidimensional phase spaces. Note that in the case that the diabatic PESs of the system are harmonic, the MS-LT-QFPE yields the same results as the HEOM for a reduced electronic system with a Brownian spectral density.[39,61] In Appendices A and B, we present a stochastic Liouville description of the (MS-)LT-QFPE and Langevin description of the LT-QFPE, respectively.

2.3. Multistate Low-Temperature Quantum Smoluchowski Equations. In this section, we present the asymptotic form of eq 11 in the Smoluchowski limit, that is, in the case $\zeta \gg \omega_0$ and ω_e, where ω_e is the characteristic

DOI: 10.1021/acs.jctc.8b01195
J. Chem. Theory Comput. 2019, 15, 2517−2534

frequency of the electronic transition dynamics. We introduce the following probability distribution in coordinate space:

$$\boldsymbol{f}^{\mathrm{d}}(q,t) \equiv \int \mathrm{d}p \boldsymbol{W}^{\mathrm{d}}(p,q,t) \tag{16}$$

In the Smoluchowski limit, the equations of motion for $\boldsymbol{f}^{\mathrm{d}}(q)$ are

$$\begin{aligned}\frac{\partial}{\partial t}\boldsymbol{f}^{\mathrm{d}}_{\vec{n}}(q,t) &= -\left[\mathcal{E}^{\mathrm{d}}(q) + \sum_k^K n_k\nu_k + \frac{\omega_0}{\zeta}(\mathcal{F}^{\mathrm{d}}(q) + \hat{\Xi}^{\mathrm{od,d}}_K(q))\right]\boldsymbol{f}^{\mathrm{d}}_{\vec{n}}(q,t) \\ &\quad - \sum_k^K \hat{\Phi}^{\mathrm{od,d}}(q)\boldsymbol{f}^{\mathrm{d}}_{\vec{n}+\vec{e}_k}(q,t) \\ &\quad - \frac{\omega_0}{\zeta}\sum_k^K n_k\nu_k\hat{\Theta}^{\mathrm{od,d}}_k(q)\boldsymbol{f}^{\mathrm{d}}_{\vec{n}-\vec{e}_k}(q,t)\end{aligned} \tag{17}$$

where

$$\mathcal{E}^{\mathrm{d}}(q)\boldsymbol{f}(q,t) \equiv \frac{i}{\hbar}(\boldsymbol{U}^{\mathrm{d}}(q)\boldsymbol{f}(q,t) - \boldsymbol{f}(q,t)\boldsymbol{U}^{\mathrm{d}}(q)) \tag{18a}$$

corresponds to the Liouville−von Neumann equation for the electronic subspace and

$$\mathcal{F}^{\mathrm{d}}(q)\boldsymbol{f}(q,t) \equiv \frac{\partial}{\partial q}\frac{1}{2}(\boldsymbol{F}^{\mathrm{d}}(q)\boldsymbol{f}(q,t) + \boldsymbol{f}(q,t)\boldsymbol{F}^{\mathrm{d}}(q)) \tag{18b}$$

is the drift term that arises from the force $\boldsymbol{F}^{\mathrm{d}}(q) \equiv -(1/\hbar)\partial\boldsymbol{U}^{\mathrm{d}}(q)/\partial q$. The operators

$$\hat{\Phi}^{\mathrm{od,d}}(q) = -\frac{\partial}{\partial q} \tag{19a}$$

and

$$\hat{\Theta}^{\mathrm{od,d}}_k(q) = \frac{2\eta_k}{\beta\hbar}\frac{\partial}{\partial q} \tag{19b}$$

represent the non-Markovian parts of the noise, while

$$\hat{\Xi}^{\mathrm{od,d}}_K(q) = -\frac{1}{\beta\hbar}\frac{\partial^2}{\partial q^2} + \sum_k^K \hat{\Phi}^{\mathrm{od,d}}(q)\hat{\Theta}^{\mathrm{od,d}}_k(q) \tag{19c}$$

represent the Markovian part of the noise. The superscript "od" means "overdamped". The derivation of eq 17 is given in section S1.C. In the case of a single-state system, the matrices $\boldsymbol{f}^{\mathrm{d}}(q,t)$, $\boldsymbol{U}^{\mathrm{d}}(q)$, and $\boldsymbol{F}^{\mathrm{d}}(q)$ reduce to scalar functions, $f(q,t)$, $U(q)$, and $F(q)$, respectively. The relationship between eq 11 and eq 17 is similar to the relationship between the Fokker−Planck (Kramer's) equation and the Smoluchowski equation.[62,63] For this reason, we refer to eq 17 as the (multistate) low-temperature quantum Smoluchowski equations ((MS-)LT-QSE), while we refer to this as the (multistate) Smoluchowski equation ((MS-)SE) in the high-temperature limit.

A quantum mechanical extension of the Smoluchowski equation valid in the low-temperature regime is known as the quantum Smoluchowski equation (QSE), which treats QLT effects in the framework of the Markovian approximation.[48,49,64−67] However, because QLT corrections are in principle non-Markovian as shown in eq 8b, when we lower the bath temperature or we study a system with high energy, the QSE becomes inaccurate. In contrast, the (MS-)LT-QSE can describe non-Markovian terms that is necessary to satisfy the QFD theorem, the (MS-)LT-QSE is applicable to a wider range of physical conditions than the QSE, as shown in Appendix C. For electron transfer problems with harmonic PESs, an extension of the Smoluchowski equation to multistate systems has been carried out as the Zusman equation (ZE).[50,51,68,69] However, the original ZE theory does not treat quantum dynamical effects from electronic states properly, as shown in Appendix D. The MS-SE can be regarded as a generalization of the ZE for arbitrary PESs with describing the quantum dynamical effects from the electric states accurately. The MS-LT-QSE can be regarded as a generalization of the MS-SE with the QLT correction terms. Several extensions of the ZE theory valid in the low-temperature regime have been carried out as the following: The generalized ZE is constructed as an extension of the quantum Smoluchowski equation to multistate systems.[70] In the modified ZE theory[52] and stochastic ZE theory,[71] the effects of non-Markovian QLT terms are incorporated using an integral-differential equation similar to that used in second-order perturbation theories and using a stochastic differential equation, respectively. In contrast, the MS-LT-QSE is a non-Markovian, nonperturbative, and deterministic approach in the framework of the HEOM formalism. Note that when the diabatic PESs of the system are harmonic, the MS-LT-QSE gives the same result as the HEOM for a reduced electronic system with an overdamped Brownian/Drude spectral density.[35,39] In Appendices A and B, we also present a stochastic Liouville description of the (MS-)LT-QSE and Langevin description of the LT-QSE, respectively.

3. NUMERICAL RESULTS

In principle, with the (MS-)LT-QFPE, we are able to calculate various physical quantities with any desired accuracy by adjusting the number of low-temperature correction terms, while the (MS-)LT-QSE is sufficient for computing physical quantities under overdamped conditions. Here, we first examine the validity of eqs 11 and 17 by presenting the results obtained from numerical integrations of these equations in the case of a Brownian oscillator, for which exact solutions are known. Then, we demonstrate the applicability of these equations by using them to compute the population dynamics and transient absorption spectrum for a multistate double-well system.

3.1. Single-State Case: Brownian Oscillator. Here, we consider the case of a single PES described by the harmonic potential

$$U(q) = \frac{\hbar\omega_0}{2}q^2 \tag{20}$$

The validity of the reduced equation of motion for a non-Markovian system can be examined by comparing the results obtained from a set of numerical tests (non-Markovian tests) to the analytically derived solution in the case of the Brownian oscillator.[32]

First, we study the equilibrium distribution function in the case of the above harmonic potential. For this PES, we have the following analytical expression for the equilibrium distribution:[47,57]

$$f(q) = \frac{1}{\sqrt{2\pi\langle q^2\rangle_{\beta,\zeta}}}e^{-q^2/2\langle q^2\rangle_{\beta,\zeta}} \tag{21}$$

Here

DOI: 10.1021/acs.jctc.8b01195
J. Chem. Theory Comput. 2019, 15, 2517−2534

$$\langle q^2\rangle_{\beta,\zeta} = \frac{2}{\pi}\int_0^\infty d\omega \tilde{C}_q(\omega) \quad (22a)$$

$$= \frac{\omega_0}{\beta\hbar}\sum_{k=-\infty}^{\infty}\frac{1}{{\omega_0}^2 + |\tilde{\nu}_k|\zeta + {\tilde{\nu}_k}^2} \quad (22b)$$

is the mean square of the coordinate q, and

$$\tilde{C}_q(\omega) = \frac{1}{2}\coth\left(\frac{\beta\hbar\omega}{2}\right)\frac{1}{\omega_0}\frac{\zeta{\omega_0}^2\omega}{({\omega_0}^2-\omega^2)^2+\zeta^2\omega^2} \quad (23)$$

is the symmetrize-correlation function of the coordinate q.

To obtain the thermal equilibrium state numerically, we integrated eqs 11 and 17 from a temporal initial state to a time sufficiently long that all of the hierarchical elements reached the steady state. For all of our computations, we fixed the oscillator frequency to $\omega_0 = 400\ cm^{-1}$. We consider the underdamped ($\zeta = 0.1\omega_0$), critically damped ($\zeta = 2\omega_0$), and overdamped cases ($\zeta = 10\omega_0$) at the temperature $\beta\hbar\omega_0 = 7.47$ ($T = 77\ K$), which is in the low-temperature regime.

Because both eqs 11 and 17 consist of sets of infinitely many differential equations, we need to truncate $\vec{n}$ to carry out numerical calculations. Here, we adopted the truncation scheme proposed in refs 72 and 73 with modifications: The hierarchy is truncated in accordance with the condition that $\vec{n}$ satisfies the relation $\delta_{\vec{n}}\omega_0/\gamma_{\vec{n}} > \delta_{tol}$, where δ_{tol} is the tolerance of the truncation, with $\gamma_{\vec{n}} \equiv \sum_k^K n_k\nu_k$ and

$$\Delta_{\vec{n}} \equiv \prod_k^K \frac{1}{n_k!}\left(\frac{\eta_k}{\eta_K}\right)^{n_k} \quad (24)$$

For details, see section S4.

Numerical calculations were carried out to integrate eqs 11 and 17 using the fourth-order low-storage Runge−Kutta (LSRK4) method.[74] The time step for the LSRK4 method was chosen between $\delta t = 0.1\times10^{-2}$ fs and $\delta t = 0.5\times10^{-2}$ fs. Uniform meshes were employed to discretize the Wigner function and probability distribution function, and the mesh sizes were set to $N_q = 64$ and $N_p = 64$ in the q and p directions, respectively. The mesh ranges of the Wigner function and probability distribution function in the q direction were chosen between $-4 \le q \le +4$ and $-12 \le q \le +12$. The mesh range of the Wigner function in the p direction was chosen between $-4 \le p \le +4$ and $-15 \le p \le +15$. The finite difference calculations for q and p derivatives in eqs 11 and 17 were performed using the central difference method with tenth-order accuracy. For the kinetic term of the Liouvillian in eq 12a, the upwind difference method with ninth-order accuracy was employed for the q derivative.[44−46,75] The Moyal products in eq 12c were evaluated using the discretized convolution representation described in refs 75−77 with modifications for multistate systems (for details of the modifications, see section S6.1). The number of QLT correction terms was chosen from $K = 3$ and 4 for the low-temperature case ($\beta\hbar\omega_0 = 7.47$ (77 K)), and $K = 2$ was employed for the high-temperature case ($\beta\hbar\omega_0 = 1.92$ (300 K)). The tolerance of the truncation was chosen between $\delta_{tol} = 10^{-4}$ and $\delta_{tol} = 10^{-6}$. In the case of $\delta_{tol} = 10^{-4}$, the number of total hierarchical elements were 34 and 14 for the low-temperature and high-temperature cases, respectively. The C++ source codes, which allow for the treatment of the phase and coordinate space dynamics with any single-state or multistate potential forms, are provided as Supporting Information. The actual numerical integrations for the present calculations were carried out using C++/CUDA codes with cuBLAS and cuFFT libraries to enhance the computational speed with graphics processing unit (GPU).

In Figure 2, we compare the analytic equilibrium distribution with that obtained from the LT-QFPE under several conditions for the system-bath coupling at $\beta\hbar\omega_0 = 7.47$. The results obtained from the LT-QFPE are overlapped to analytically exact solutions. In the numerical calculation, the larger number K we used, the more accurate results we had.

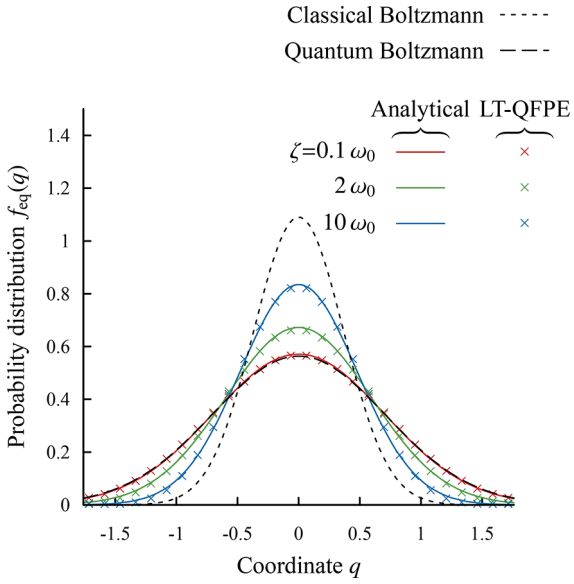

Figure 2. Equilibrium distributions for a harmonic oscillator in the underdamped ($\zeta = 0.1\omega_0$), critically damped ($\zeta = 2\omega_0$), and overdamped ($\zeta = 10\omega_0$) cases at low-temperature, $\beta\hbar\omega_0 = 7.47$ ($T = 77$ K). The red, green, and blue curves represent the analytically derived solutions, eq 21, and the red, green, and blue symbols represent the numerical results obtained with the LT-QFPE. The classical and quantum equilibrium distributions of the system without a heat bath are also presented as the dotted and dashed curves, respectively.

In the case of a weak interaction, both the numerical and analytical forms are closer to that for the isolated harmonic oscillator, which is given by eq 21 with $\langle q^2\rangle_{\beta,0} = (1/2)\coth(\beta\hbar\omega_0/2)$. This expression can also be derived from the Boltzmann summation of the eigenstates.

As mentioned above, the mean-square momentum, $\langle p^2\rangle$, diverges in the present Ohmic case.[47,57] This is because high frequency quantum noise destroys the quantum coherence between the "bra" and "ket" wave functions, which results in the condition $\rho(z,z') = 0$ for $z \ne z'$. As a result, the Wigner distribution function in momentum space, which is the Fourier transform of the quantum coherence $r \equiv z-z'$, is flat in this case (see section S5). However, even in such situations, we can use the Wigner function, because the dynamics of the system are controlled by the low-frequency Matsubara terms or the low-frequency QLT correction terms.

In Figure 3, we plot stable solutions for the Wigner distribution function calculated with the LT-QFPE using several values for the number of QLT correction terms. It is seen that the width of Wigner distributions ($\propto\langle p^2\rangle$) increases as the number of QLT correction terms increases, while the q probability distributions converge to on the analytically derived solution. The Gaussian-like profile in the p direction arises

DOI: 10.1021/acs.jctc.8b01195
J. Chem. Theory Comput. 2019, 15, 2517−2534

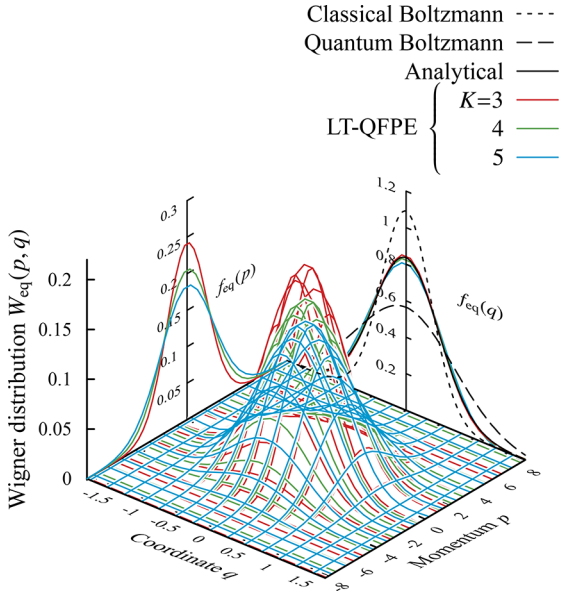

Figure 3. Wigner distribution function for the equilibrium state of a harmonic oscillator in the overdamped case ($\zeta = 10\omega_0$) at $\beta\hbar\omega_0 = 7.47$ ($T = 77$ K) using several values of the number of QLT correction terms ($K = 3$, 4, and 5). The reduced distributions $f(q)$ and $f(p) \equiv \int dq\, W(p,q)$ are also displayed.

from QLT correction terms for finite K. Although we observe the larger flat distribution for larger K, we can still use the Wigner function by ignoring these contribution for the calculation of the nondiverging physical variables. This is the reason that we can calculate the physical variable using Wigner distribution, while $\langle p^2 \rangle$ diverges with $K \to \infty$.

We next study the symmetrized correlation function of the system coordinate, defined as

$$C_q(t) \equiv Tr\left\{ z\mathcal{G}_{tot}(t)\frac{z+z'}{2}\rho_{tot}^{eq}(z, z', \vec{x}, \vec{x}') \right\} \tag{25}$$

where $\mathcal{G}_{tot}(t)$ is Green's function for the total system and $W^{eq}(p, q, \vec{x}, \vec{x})$ is the stationary solution of $\mathcal{G}(t)$. In the HEOM formalism, the time evolution of the total system, described by $\rho_{tot}(z, z', \vec{x}, \vec{x}', t)$, is replaced by that of the hierarchical elements, described by $\rho_H(z, z', t) \equiv \{\rho_{\vec{n}}(z, z', t) | \vec{n} \in \mathbb{N}^K\}$. It has been found that these yield the same reduced dynamics in the system subspace.[32,78] After the Wigner transformation, eq 25 is evaluated as

$$C_q(t) = \int dp \int dqq\{\mathcal{G}_H(t) q W_H^{eq}(p, q)\}|_{\vec{n}=\vec{0}} \tag{26}$$

where $\mathcal{G}_H(t)$ is Green's function evaluated from eq 11 or 17, and $W_H^{eq}(p,q)$ is the stationary solution of $\mathcal{G}_H(t)$. We define the Fourier transform of eq 25 as

$$C_q(\omega) \equiv \int_0^\infty dt C_q(t) \cos \omega t \tag{27}$$

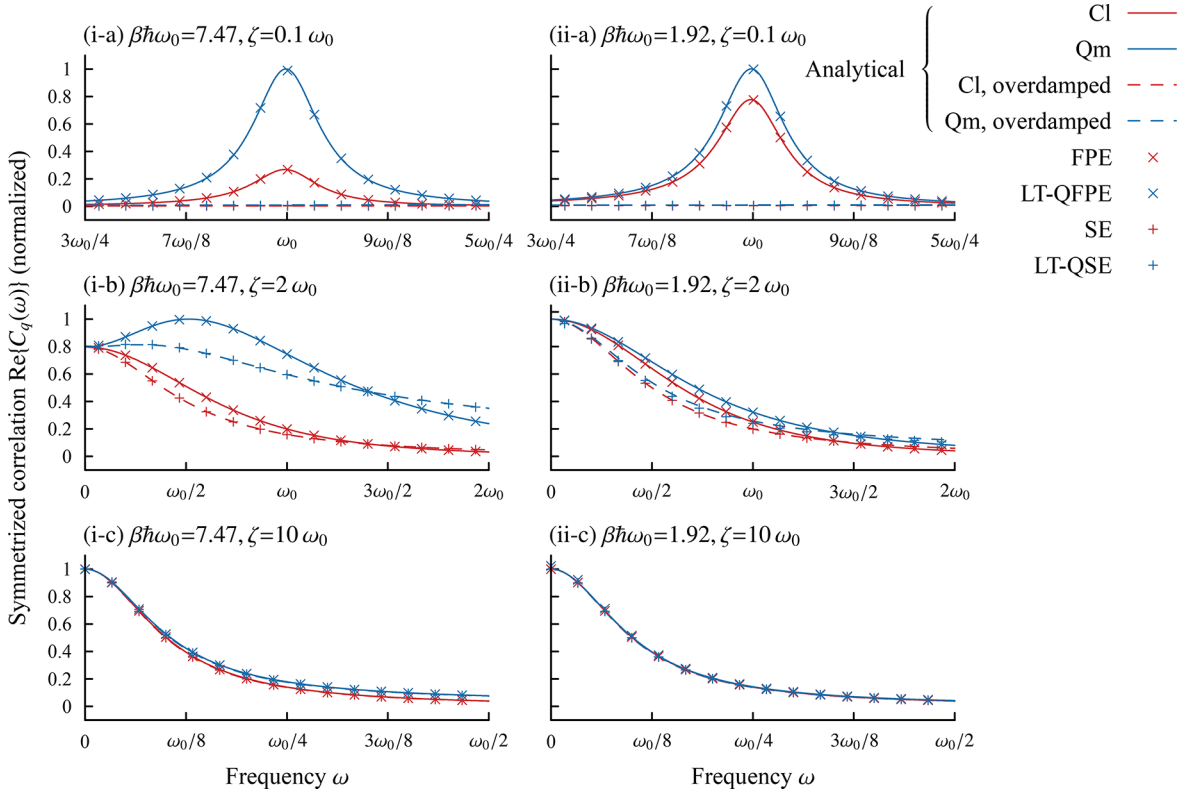

Figure 4. Symmetrized correlation function given in eq 25 for a harmonic oscillator under (a) underdamped ($\zeta = 0.1\omega_0$), (b) critically damped ($\zeta = 2\omega_0$), and (c) overdamped conditions ($\zeta = 10\omega_0$) in (i) low-temperature ($\beta\hbar\omega_0 = 7.47$ (77 K)) and (ii) high-temperature ($\beta\hbar\omega_0 = 1.92$ (300 K)) cases. The solid and dotted curves were calculated from eqs 23 and 28 for the classical (red) and quantum (blue) cases, respectively. The values plotted here are normalized with respect to the maximum of eq 23. The LT-QFPE and LT-QSE results are denoted by the blue symbols, respectively, while the FPE and SE results are denoted by the red symbols. Note that QFPE and the classical Fokker–Planck equation (FPE) are equivalent in the case of a harmonic PES.

DOI: 10.1021/acs.jctc.8b01195
J. Chem. Theory Comput. 2019, 15, 2517–2534

In the quantum case, eq 27 can be analytically evaluated as eq 23. Under the condition $\zeta \gg \omega_0$, this function asymptotically approaches[38,79]

$$\tilde{C}_q^{\zeta \gg \omega_0}(\omega) = \frac{1}{2}\coth\left(\frac{\beta\hbar\omega}{2}\right)\frac{1}{\omega_0}\frac{\tilde{\gamma}\omega}{\omega^2 + \tilde{\gamma}^2} \tag{28}$$

where $\tilde{\gamma} \equiv \omega_0^2/\zeta$. The classical high-temperature limit of the above result is obtained by replacing $\coth(\beta\hbar\omega/2)$ with $2/\beta\hbar\omega$. In Figure 4, we depict the symmetrized-correlation function calculated under several damping conditions in (i) low temperature ($\beta\hbar\omega_0 = 7.47$) and (ii) high temperature ($\beta\hbar\omega_0 = 1.92$) cases. As seen there, the numerical results obtained from eqs 11 and 17 are close to the exact analytical solutions. Generally, in the HEOM formalism, we are able to obtain as accurate results as we need by employing larger hierarchical space (i.e., by increasing K and by decreasing δ_{tol}). It should be noted that, although the LT-QSE well predicts the quantum dynamics under strong friction, the stable solution of the LT-QSE depend upon the number of QLT correction terms. As shown in Appendix C, because the analytical solution for the overdamped case, eq 28, also diverges under the infinite summation of the Matsubara frequencies, careful verification is important when we use the LT-QSE to calculate observable strongly depend on the equilibrium distribution.

As shown in this section, the LT-QFPE and LT-QSE can describe accurate dynamics with a properly truncated hierarchical space. This finding is important for numerical calculations. As shown in Appendix B, the LT-QFPE and LT-QSE are equivalent to the Langevin expressions for a single harmonic potential case. As analytically calculated symmetrized correlation functions from the Langevin equations indicate, we can obtain eqs 23 and 28 from the present approach, under $\delta_{\mathrm{tol}} \to 0$ and $K \to \infty$. This result demonstrates the reliability of the LT-QFPE and LT-QSE theories.

3.2. Multistate Case: Double-Well PESs with Gaussian Adiabatic Coupling. Next, we present our numerical results for multistate systems. For convenience, we describe our system using adiabatic electronic states, $|\Phi_a(z)\rangle$. In the following, a, b, and c refer to adiabatic electronic states, and j, k, and l refer to diabatic electronic states.

3.2.1. Adiabatic and Diabatic Bases. The ath adiabatic electronic state is an eigenfunction of the time-independent Schrödinger equation, and thus we have

$$\hat{U}(z)|\Phi_a(z)\rangle = U_a^{\mathrm{a}}(z)|\Phi_a(z)\rangle \tag{29}$$

where $\hat{U}(z) \equiv \sum_{j,k}|j\rangle U_{jk}^{\mathrm{d}}(z)\langle k|$ and $U_a^{\mathrm{a}}(z)$ is the ath adiabatic Born−Oppenheimer (BO) PES. The diabatic and adiabatic states are related through the transformation matrix given by

$$Z_{ja}(z) \equiv \langle j|\Phi_a(z)\rangle \tag{30}$$

We introduce the unitary matrix $\mathbf{Z}(z)$ defined as $\{\mathbf{Z}(z)\}_{ja} = Z_{ja}(z)$, which satisfies the relation $\mathbf{Z}(z)^\dagger\mathbf{Z}(z) = \mathbf{Z}(z)\mathbf{Z}(z)^\dagger = \mathbf{1}$. Then, eq 29 can be expressed in diagonal matrix form as

$$\mathbf{Z}(z)^\dagger\mathbf{U}^{\mathrm{d}}(z)\mathbf{Z}(z) = \mathbf{U}^{\mathrm{a}}(z) \tag{31}$$

where $\{\boldsymbol{U}_{\mathrm{a}}(z)\}_{ab} \equiv \delta_{ab}U_{\mathrm{a}}^a(z)$, and δ_{ab} is the Kronecker delta.

In adiabatic representations of kinetic equations, nonadiabatic couplings between adiabatic states are characterized by the nonadiabatic coupling matrix, $\boldsymbol{d}(z)$, expressed in terms of the first-order derivative of the coordinate as[80,81]

$$\{\boldsymbol{d}(z)\}_{ab} = d_{ab}(z) \equiv \langle\Phi_a(z)|\frac{\partial}{\partial z}|\Phi_b(z)\rangle \tag{32a}$$

The nonadiabatic coupling matrix, $\boldsymbol{d}$, is skew-Hermitian (i.e., $\boldsymbol{d}^\dagger = -\boldsymbol{d}$). This matrix can also be expressed in terms of $\mathbf{Z}(z)$ as

$$\boldsymbol{d}(z) = \mathbf{Z}(z)^\dagger\frac{\partial}{\partial z}\mathbf{Z}(z) \tag{32b}$$

and therefore we have

$$\mathbf{Z}(z) = \mathbf{Z}(-\infty)\overrightarrow{\exp}\left(\int_{-\infty}^{z} dz'\boldsymbol{d}(z')\right) \tag{33}$$

where $\overrightarrow{\exp}$ is the ordered exponential in coordinate space. Thus, the transformation matrix, eq 30, can be constructed from $\boldsymbol{d}(z)$, and hence the diabatic PESs can be obtained from the adiabatic PESs using the inverse of the transformation in eq 31.

If necessary, we can introduce the nonadiabatic coupling matrix of the second-order, defined as

$$\{\boldsymbol{h}(z)\}_{ab} = h_{ab}(z) \equiv \langle\Phi_a(z)|\frac{\partial^2}{\partial z^2}|\Phi_b(z)\rangle \tag{34a}$$

which can be constructed from $\boldsymbol{d}(z)$ as

$$\boldsymbol{h}(z) = \mathbf{Z}(z)^\dagger\frac{\partial^2}{\partial z^2}\mathbf{Z}(z) = \frac{\partial\boldsymbol{d}(z)}{\partial z} + \boldsymbol{d}(z)^2 \tag{34b}$$

Next, we introduce the reduced density matrix in the adiabatic representation, defined as

$$\rho_{ab}^{\mathrm{a}}(z, z', t) \equiv \langle\Psi_a(z)|\hat{\rho}(z, z', t)|\Psi_b(z')\rangle \tag{35}$$

where the diagonal element $\rho_{aa}^{\mathrm{a}}(z, z, t)$ and the off-diagonal element $\rho_{ab}^{\mathrm{a}}(z, z', t)$ $(a \neq b)$ represent the population of $|\Phi_a(z)\rangle$ and the coherence between $|\Phi_a(z)\rangle$ and $|\Phi_b(z')\rangle$, respectively. The adiabatic representation of the density matrix, $\{\boldsymbol{\rho}^{\mathrm{a}}(z, z', t)\}_{ab} = \rho_{ab}^{\mathrm{a}}(z, z', t)$, can be obtained from $\boldsymbol{\rho}^{\mathrm{d}}(z, z', t)$ through application of the transformation matrix $\mathbf{Z}(z)$ as

$$\boldsymbol{\rho}^{\mathrm{a}}(z, z', t) = \mathbf{Z}(z)^\dagger\boldsymbol{\rho}^{\mathrm{d}}(z, z', t)\mathbf{Z}(z') \tag{36}$$

This representation is related to the Wigner representation as

$$\boldsymbol{W}^{\mathrm{a}}(p, q, t) \equiv \frac{1}{2\pi}\int \mathrm{d}r e^{-ipr}\boldsymbol{\rho}^{\mathrm{a}}\left(q + \frac{r}{2}, q - \frac{r}{2}\right) \tag{37}$$

Although we can construct the equations of motion for $\boldsymbol{W}^{\mathrm{a}}(p,q,t)$ directly, the numerical integrations are complicated, because the number of terms that include the Moyal product becomes large (see Appendix E). For this reason, we integrate the equations of motion in the diabatic representation. After obtained the numerical results, we convert these to the adiabatic representation.

3.2.2. Tilted Double-Well Model. As a schematic model for IC in a photoisomerization process, we adopt the following tilted double-well adiabatic ground BO PES:

$$U_g^{\mathrm{a}}(q) = \frac{\hbar\omega_0}{2{L_0}^2}q^2\left(q^2 - \frac{{L_0}^2}{2}\right) + \frac{\Delta E}{L_0}q \tag{38a}$$

Here, L_0 and ΔE are the displacement between the wells and the difference between their energies, respectively. We use the following harmonic adiabatic excited BO PES:

DOI: 10.1021/acs.jctc.8b01195
J. Chem. Theory Comput. 2019, 15, 2517−2534

$$U_e^{\mathrm{a}}(q) = \frac{\hbar\omega_e^{\ 2}}{2\omega_0}(q - q^\dagger)^2 + U_g^{\mathrm{a}}(q^\dagger) + E_{\mathrm{gap}}^{e-g} \tag{38b}$$

Here, ω_e, $q^\dagger$, and E_{gap}^{e-g} are the vibrational characteristic frequency in the excited state, the position of the crossing region, and the energy gap between the ground and excited BO PES in the crossing region, respectively.

We assume that the nonadiabatic coupling has the Gaussian form

$$d_{eg}(q) = -d_{ge}(q) = \sqrt{\frac{\pi}{8\sigma^{\dagger 2}}}\, e^{-(q-q^\dagger)^2/2\sigma^{\dagger 2}} \tag{39}$$

and $d_{gg}(q) = d_{ee}(q) = 0$, where $\sigma^\dagger$ is the width of the crossing region. The integral of $d_{eg}(q)$ is given by

$$D_{eg}(q) \equiv \int_{-\infty}^{q} \mathrm{d}q'\, d_{eg}(q') = \frac{\pi}{4}\mathrm{erfc}\left(-\frac{q - q^\dagger}{\sqrt{2}\,\sigma^\dagger}\right) \tag{40}$$

where $\mathrm{erfc}(x) \equiv 1 - \mathrm{erf}(x)$ is the complementary error function. Because $d_{eg}(q)$ is normalized with respect to $D_{eg}(\infty) = \pi/2$, the adiabatic bases are exchanged with the change of position from $z = -\infty$ to $z = +\infty$.

Although we can construct the MS-LT-QFPE and their variant equations in the adiabatic representation (see Appendix E), in the present study, we performed the numerical calculation using the diabatic representation, because in this case, the equations are simpler and easier to solve. Then, after we obtained the numerical results, we carried out the inverse transformation to convert these to the adiabatic representation. We employ the diabatic basis defined as $|0\rangle \equiv |\Phi_g(-\infty)\rangle$ and $|1\rangle \equiv |\Phi_e(-\infty)\rangle$. Then eq 33 is solved as

$$\mathbf{Z}(q) = \begin{pmatrix} \cos D_{eg}(q) & -\sin D_{eg}(q) \\ +\sin D_{eg}(q) & \cos D_{eg}(q) \end{pmatrix} \tag{41}$$

and the diabatic PESs and coupling are given by

$$\begin{cases} U_{00}^{\mathrm{d}}(q) = \dfrac{U_e^{\mathrm{a}}(q) + U_g^{\mathrm{a}}(q)}{2} - \cos(2D_{eg}(q))\dfrac{U_e^{\mathrm{a}}(q) - U_g^{\mathrm{a}}(q)}{2} \\ U_{11}^{\mathrm{d}}(q) = \dfrac{U_e^{\mathrm{a}}(q) + U_g^{\mathrm{a}}(q)}{2} + \cos(2D_{eg}(q))\dfrac{U_e^{\mathrm{a}}(q) - U_g^{\mathrm{a}}(q)}{2} \\ U_{10}^{\mathrm{d}}(q) = U_{01}^{\mathrm{d}}(q) = -\sin(2D_{eg}(q))\dfrac{U_e^{\mathrm{a}}(q) - U_g^{\mathrm{a}}(q)}{2} \end{cases} \tag{42}$$

Figure 5 presents the adiabatic BO PESs and diabatic PESs for the parameter values listed in Table 2.

We set the initial distribution as

$$W_{ee}^{\mathrm{a}}(p, q, 0) = \frac{1}{\mathcal{Z}} e^{-\tanh(\beta\hbar\omega_0/2)[p^2 + (q-q_{\mathrm{i}})^2]} \tag{43}$$

and as $W_{gg}^{\mathrm{a}}(p, q, 0) = W_{eg}^{\mathrm{a}}(p, q, 0) = W_{ge}^{\mathrm{a}}(p, q, 0) = 0$ in eq 43, where $q_{\mathrm{i}} = -L_0/2$ and $\mathcal{Z}$ is the partition function. This is the Wigner transformation of the Boltzmann distribution for the harmonic oscillator centered at $q = q_{\mathrm{i}}$. In this demonstration, we ignore the initial correlation at $t = 0$.

We performed the numerical calculations to integrate equations of motion using the finite difference method with mesh sizes $N_q = 256$ and $N_p = 64$ and mesh ranges $-12 \le q \le +12$ and $-12 \le p \le +12$. The other calculation conditions were the same as in section 3.1. For comparison, we display the results calculated using the fewest switch surface hopping (FSSH)[26,82] and Ehrenfest methods[80,81] with a classical Markovian Langevin force under the same conditions. In both methods, the adiabatic electronic basis was employed. In the Ehrenfest methods, the state of the system is described using the electronic density matrix (or the electronic wave function), $\boldsymbol{\rho}^{\mathrm{el}}(t)$, and a trajectory, $\{p(t), q(t)\}$, which is determined following the mean-field force calculated from the electronic PESs (i.e., averaged force from the populations in $\boldsymbol{\rho}^{\mathrm{el}}(t)$). In the FSSH methods, the state is also described using $\boldsymbol{\rho}^{\mathrm{el}}(t)$, but its trajectory, $\{p(t), q(t)\}$, now follows the force calculated from the active PES, $U_{\lambda(t)}^{\mathrm{a}}(q)$, where $\lambda(t)$ is a

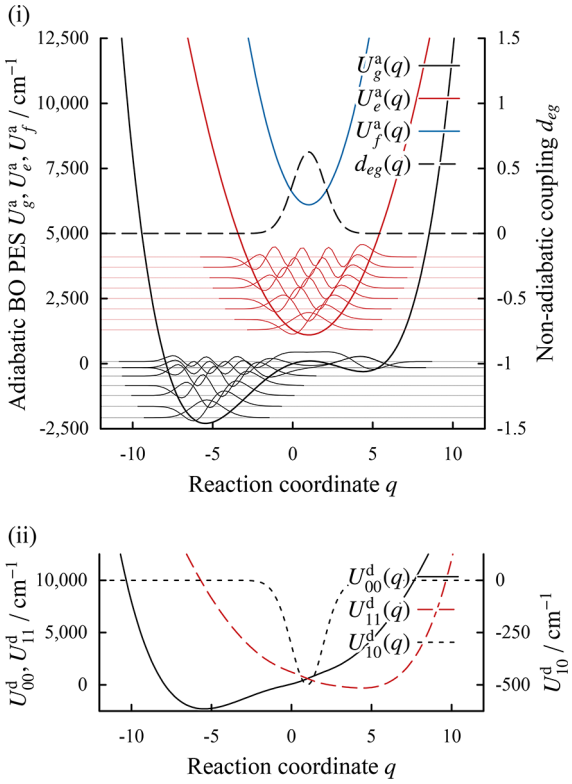

Figure 5. (i) The adiabatic ground BO PES (black solid curve), excited BO PES (red solid curve), and nonadiabatic coupling (black dashed curve) given by eqs 38a, 38b, and 39 are depicted for the parameter values given in Table 2. The blue solid curve represents the second excited BO PES. The first eight vibrational eigenfunctions for the ground and first excited BO PESs are also plotted. (ii) The diabatic 00 PES (black solid curve), diabatic 11 PES (red dashed curve), and the diabatic 10 coupling (black dotted curve) for the case of panel i.

Table 2. Parameter Values for the Numerical Tests

symbol	value
ω_0	400 cm^{-1}
ω_e	ω_0
ω_f	$1.5\omega_0$
L_0	10
ΔE	2000 cm^{-1}
E_{gap}^{e-g}	1000 cm^{-1}
E_{gap}^{f-e}	5000 cm^{-1}
$q^\dagger$	1
$\sigma^\dagger$	1

DOI: 10.1021/acs.jctc.8b01195
J. Chem. Theory Comput. 2019, 15, 2517−2534

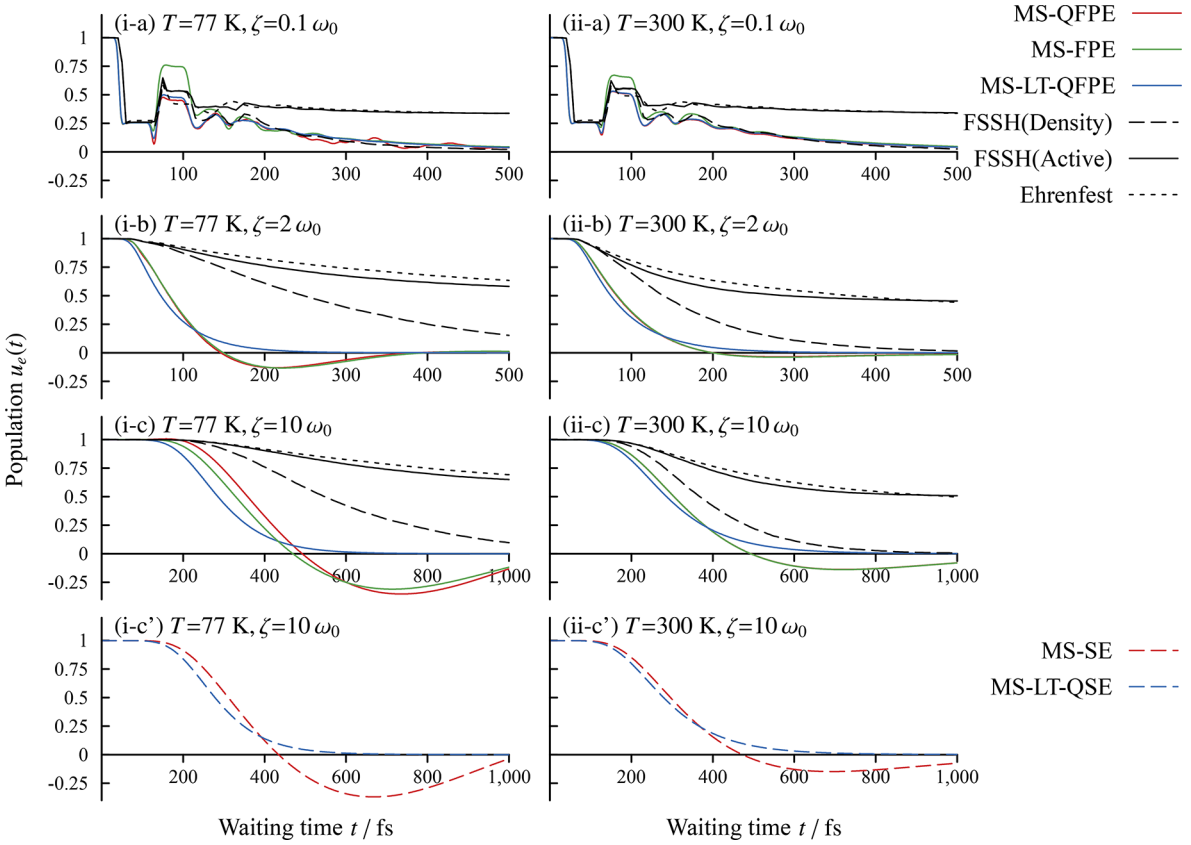

Figure 6. Time evolution of the excited population in the adiabatic state $|\Phi_e^a\rangle$ under (a) underdamped ($\zeta = 0.1\omega_0$), (b) critically damped ($\zeta = 2\omega_0$), and (c) overdamped conditions ($\zeta = 10\omega_0$) in the (i) low-temperature (77 K) and (ii) high-temperature (300 K) cases, respectively. The red and blue solid curves were calculated using the MS-QFPE and MS-LT-QFPE, respectively. The green solid curves represent the MS-FPE results. These were derived using the first-order Moyal-truncated Liouvillian, which is equivalent to the mixed quantum-classical Liouvillian.[20,21] The black solid and dotted curves are the ensemble averages of the excited state population of the electronic density matrix, $\rho_{ee}^{el}(t)$, calculated in the FSSH and Ehrenfest cases, respectively. The black dashed curves are the excited population, $\overline{u}_{\lambda(t)=e}(t)$, in the FSSH (active) case. Panels i-c′ and ii-c′ correspond to the Smoluchowski limit, which can be evaluated from eq 17.

randomly changing index (i.e., g or e) in time whose hopping rate is calculated using $\boldsymbol{\rho}^{el}(t)$. In each case, the time evolution of the particle trajectories under the Langevin force was calculated using the Vanden−Eijnden−Ciccotti methods.[83] The time evolution of $\boldsymbol{\rho}^{el}(t)$ was calculated by the numerical integration of the Schrödinger equation (NISE) method,[84,85] in which the coefficients of the time evolution operator of the electronic density matrix were held constant during each time step evaluation. We used $\delta t = 0.1$ fs as the time step for the integrations using the FSSH and Ehrenfest methods, and we employed $N \simeq 10\,000$ trajectories for the average calculations.

3.2.3. Population Dynamics. In Figure 6, we present plots of the excited population in the adiabatic representation defined as

$$u_e(t) \equiv \int \mathrm{d}p \int \mathrm{d}q W_{ee}^{a}(p, q, t) \tag{44}$$

In the FSSH and Ehrenfest cases, we defined $u_e(t)$ as an ensemble average of $\rho_{ee}^{el}(t)$ for all trajectories. In the FSSH (active) case, we further introduced the excited population, $\overline{u}_{\lambda(t)=e}(t)$, calculated as an ensemble average of the population with the active PES index $\lambda(t) = e$ for all trajectories.

As demonstrated in section 3.1, the MS-LT-QFPE is numerically accurate, and therefore, the calculated results obtained with these equations can be used as a reference to verify other results from different formalisms. We now discuss the numerical results. A wavepacket centered at $q = q_i$ in the excited state as the initial state. The wavepacket then moves in the direction of the crossing region, that is, near $q = q^{\dagger}$. Then the population of $|\Phi_e(q)\rangle$ decreases due to the nonadiabatic transition. In the case that ζ is sufficiently small, the de-excited wavepacket moves among the double minima of the adiabatic ground state PES while maintaining a large kinetic energy, and it traverses the crossing region repeatedly through nonadiabatic transitions. As a result, oscillatory behavior is observed in Figure 6i-a and 6ii-a. As the coupling constant ζ increases, the wavepacket motion becomes slower, and the population of $|\Phi_e(q)\rangle$ decays more slowly. While classical treatments of the heat bath produce pathological negative populations (red and green curves), in particular in the low temperature case, the presently investigated equations of motion, eqs 11 and 17, accurately describe the population dynamics (the blue lines). This demonstrates the importance of the QLT correction terms.

While the results obtained with the FSSH and Ehrenfest methods do not exhibit negative populations because of the assumptions for a decomposition of the distribution function into the trajectories, they do differ significantly from both the quantum (MS-LT-QFPE) and semiclassical (MS-FPE) results, particularly in the low temperature case. Because the FSSH and Ehrenfest methods were originally developed to study isolated systems, which have a few degrees of freedom, these

DOI: 10.1021/acs.jctc.8b01195
J. Chem. Theory Comput. 2019, 15, 2517−2534

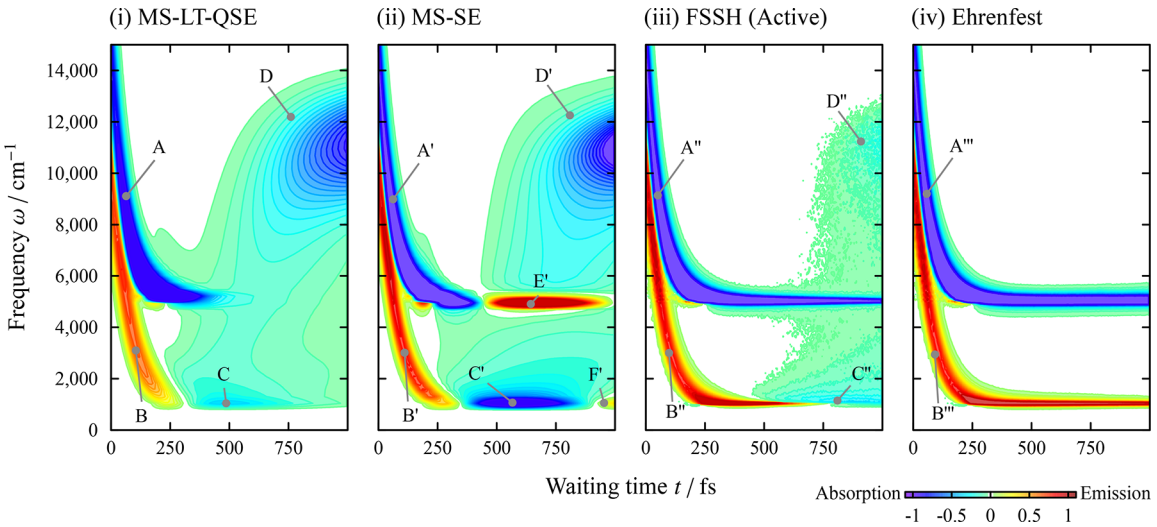

Figure 7. Transient absorption spectra, $I^{TA}(\omega,t)$, calculated in the overdamped low-temperature case ($\zeta = 10\omega_0$ and $T = 77$ K). The results were obtained using the (i) MS-LT-QSE, (ii) MS-SE, and (iii) FSSH, and (iv) Ehrenfest methods, respectively. In the FSSH method, the effects of the nonadiabatic transition dynamics during waiting time was taken into account using the ensemble average of the active PES index, $\overline{u}_{\lambda(t)=e}(t)$. The red and blue regions represent emission and absorption, respectively. The values are normalized with respect to the maximum of the MS-LT-QSE calculation at $t = 0$ fs.

methods may not be proper for calculations of systems in dissipative conditions that are essentially many-body problem when we include the bath degrees of freedom. It should be noted that, in the FSSH results, $u_e(t)$ and $\overline{u}_{\lambda(t)=e}(t)$ disagrees, while both correspond the electronic excited state. The similar disagreement is reported in ref 86.

Note that, as the coupling constant ζ increases, the results obtained from the quantum Liouvillian (red curves) and semiclassical Liouvillian (green curves) treatments of the PES become similar. This is because the higher-order differential operators in the Moyal products vanish in the overdamped limit, as shown in the construction of the LT-QSE (see section S1.C). Moreover, when the energy gap between the ground and excited states in the crossing region is small, the negative population of the semiclassical results is suppressed. This is because, the characteristic frequency of the electronic transition dynamics becomes small in such situation, and therefore the high-temperature approximation of the bath works well, as the authors' previous investigation for conical intersection problem.[20]

3.3. Transient Absorption Spectra. The presently investigated formalisms are capable of calculating nonlinear response functions. By calculating the transient absorption spectrum, here we demonstrate the importance of the QLT correction terms for nonlinear optical spectra. In order to include an excited state absorption (ESA) process, we add a second excited state, $|\Phi_f(q)\rangle$, with the PES

$$U_f^a(q) = \frac{\hbar\omega_f^2}{2\omega_0}(q - q^\dagger)^2 + U_e^a(q^\dagger) + E_{\mathrm{gap}}^{e-f} \tag{45}$$

to the present model. Because we assume $d_{fg}(q) = d_{fe}(q) = 0$, a spontaneous transition between $|\Phi_f(q)\rangle$ and the subspace $\{|\Phi_g(q)\rangle, |\Phi_e(q)\rangle\}$ is prohibited. Thus, only optically stimulated transitions between $|\Phi_g(q)\rangle$and $|\Phi_e(q)\rangle$ occur. The diabatic PESs of this three-state system are those given in eq 42, along with $U_{22}(q) = U_f(q)$, $U_{20}(q) = U_{21}(q) = 0$.

The transient absorption (TA) spectrum from the initial state eq 43 is given by[19]

$$I^{TA}(\omega, t) \equiv \omega Im \int_0^\infty d\tau e^{i\omega\tau} R^{TA}(\tau, t) \tag{46}$$

where

$$R^{TA}(\tau, t) \equiv Tr_S\left\{\boldsymbol{\mu}^d(q) Tr_B\left\{\mathcal{G}_{tot}(\tau)\frac{i}{\hbar}\boldsymbol{\mu}^d(q)^\times \mathcal{G}_{tot}(t) \times (\boldsymbol{W}^d(p, q, 0) \otimes \rho_B^{eq}(\vec{x}, \vec{x}'))\right\}\right\} \tag{47}$$

is the response function of the TA and $\{\boldsymbol{\mu}^d(q)\}_{jk} = \langle j|\hat{\mu}(q)|k\rangle$ is the dipole operator in the matrix representation. Here, $A^\times B \equiv AB - BA$ is the commutator and

$$Tr_S\{\ldots\} \equiv \int dp \int dq \sum_j \{\ldots\}_{jj} \tag{48}$$

is the trace over the system subspace. In the HEOM formalism, eq 47 becomes

$$R^{TA}(\tau, t) = Tr_S\left\{\boldsymbol{\mu}^d(q)\left\{\mathcal{G}_H(\tau)\frac{i}{\hbar}\boldsymbol{\mu}^d(q)^\times \mathcal{G}_H(t) \times \boldsymbol{W}_H^d(p, q, 0)\right\}|_{\vec{n}=\vec{0}}\right\} \tag{49}$$

where $\boldsymbol{W}_H^d(p, q, 0) \equiv \{\boldsymbol{W}_{\vec{n}}^d(z, z', t)|\vec{n} \in \mathbb{N}^K\}$ is initialized as $\boldsymbol{W}_{\vec{n}}^d(p, q, 0) = \boldsymbol{W}^d(p, q, 0)$ for $\vec{n} = \vec{0}$ and $\boldsymbol{W}_{\vec{n}}^d(p, q, 0) = 0$ otherwise.

Hereafter, for $\hat{\mu}(q)$, we assume the form $\hat{\mu}(q) = |\Phi_e(q)\rangle\langle\Phi_g(q)| + |\Phi_f(q)\rangle\langle\Phi_e(q)| + c.c.$ While $\hat{\mu}(q)$ may induce nonvertical transitions among adiabatic electronic states, here we consider the vertical transition only for simplicity (i.e., the laser interaction is described by the commutator, $\boldsymbol{\mu}^a(p, q)^\times \boldsymbol{W}^a(p, q)$ among the electronic states). Note that because the distribution, eq 43, is set in the excited state at the initial time, ground state bleaching (GSB) is not observed.

Figure 7 displays the calculated results in the overdamped case at $T = 77$ K. Here, the parameter values are the same as in Figure 6i-c′. For comparison, we display the TA spectra obtained using the FSSH and Ehrenfest methods with a classical Markovian Langevin force under the same conditions.

DOI: 10.1021/acs.jctc.8b01195
J. Chem. Theory Comput. 2019, 15, 2517−2534

As shown in Figure 6, nonadiabatic transitions in the FSSH and Ehrenfest calculations are slow. This is reflected by very sharp peaks in the TA spectra. To avoid numerical errors in the computation of the Fourier transform due to these sharp peaks, we employed an exponential filter, $\exp(-\tau/\tau_d)$, with decay time constant τ_d = 200 fs in the all calculations. The procedure of calculating nonlinear response functions using the FSSH and Ehrenfest methods following that for the two-dimensional electronic spectra given in ref 86 is presented in section S6.2.

To carry out FSSH calculations, the effects of the nonadiabatic transition dynamics during waiting time was taken into account using the ensemble average of the active PES index, $\overline{u}_{\lambda(t)=e}(t)$ (i.e., using the auxiliary wave function given in ref 86).

First, we discuss the TA spectrum plotted in Figure 7i . At t = 0, ESA and stimulated emission (SE) are observed at frequencies corresponding to the Franck−Condon point, $U_f(q_i) - U_e(q_i)$ = 14 000 cm^{-1} and $U_e(q_i) - U_g(q_i)$ = 10 552 cm^{-1}, respectively. The ESA signals is labeled "A" and the SE signal is labeled "B". Because both $U_f(q) - U_e(q)$ and $U_e(q) - U_g(q)$ decrease in accordance with the wavepacket motion from $q = q_i$ to $q = z^\dagger$, the ESA and SE peaks move toward the frequencies $\omega = U_f(q^\dagger) - U_e(q^\dagger) = E_{gap}^{f-e}$ = 5000 cm^{-1} and $U_f(q^\dagger) - U_e(q^\dagger) = E_{gap}^{e-g}$ = 1000 cm^{-1} as functions of time, respectively. The intensity of the ESA signal decreases because of the de-excitation from $|\Phi_e(q)\rangle$ to $|\Phi_g(q)\rangle$. The intensity of the SE signal also decreases, and becomes zero near t = 300 fs, because the SE from $|\Phi_e(q)\rangle$ and the absorption from $|\Phi_g(q)\rangle$ cancel each other. Then, the absorption signal from the crossing region labeled "C" appears and the position of the peak moves toward the resonant frequency of the product ground state labeled "D", following the wavepacket motion.

In Figure 7ii, the positive peak labeled E′ appears at $\omega = E_{gap}^{f-e}$ after t = 400 fs. Its appearance is due to the violation of the positivity of the excited state population of $|\Phi_e(q^\dagger)\rangle$; the E′ peak in ESA signal arises from a negative population of $|\Phi_e\rangle$, which is observed as emission. The negative population of $|\Phi_e(q^\dagger)\rangle$ also appears as an absorptive contribution in the SE, and the intensity of the negative peak labeled C′ is enhanced. When this negative population propagates to the $|\Phi_g(q^\dagger)\rangle$ state, the absorption from this state is observed as the emission spectrum labeled F′. These results indicate that the classical treatment does not have the capability to predict optical signals, in particular in the low-temperature regime.

In Figure 7iii and 7iv, the calculated results from the phenomenological FFSH and Ehrenfest approaches are presented. These results do not agree with the MS-LT-QSE results not only quantitatively but also qualitatively, in particular in the Ehrenfest case. This is due to the poor estimation of nonadiabatic transition rate in these two approaches, as illustrated in Figure 6. Although the MS-SE approach exhibits unphysical emission or absorption peaks, the MS-SE result is closer to the accurate MS-LT-QSE results than the FSSH and Ehrenfest results. This indicates that the MS-SE approach is physically more consistent than the FSSH and Ehrenfest approaches, even the positivity problem occurs. Although the FSSH and Ehrenfest approaches are simple and easy to implement molecular dynamics simulations, the verification of the calculated results, in particular for calculation of nonlinear response function, should be made before comparing the experimental results. Note that, when we calculate the effects of the nonadiabatic transition dynamic using the ensemble average of the electronic density matrix (i.e., using the primary wave function given in ref 86), the FSSH method produces a similar spectrum to the Ehrenfest result.

4. CONCLUSION

In this Article, we investigated (MS-)LT-QFPE and (MS-)LT-QSE that include QLT correction terms to satisfy the QFD theorem. The (MS-)LT-QFPE and (MS-)LT-QSE were rigorously derived from path integral formalism. We found that the (MS-)LT-QFPE can be used to obtain correct numerical descriptions of dynamics of a system coupled to an Ohmic bath when the QLT correction terms are treated properly, even in the strong coupling, low-temperature regime. In the overdamped case, we can further reduce the momentum degrees of freedom from these equations, thereby obtaining the (MS-)LT-QSE. Although the applicability of these equations is limited to the Ohmic case, they are significantly less computationally intensive than (MS-)QHFPE approaches in particular for the case of (MS-)LT-QSE. Moreover, because structures of the PESs play essential roles in nonadiabatic transition phenomena, and because the difference between the Markovian and non-Markovian noise cases is minor, the present formalism is sufficient for studying nonadiabatic transition phenomena. Applications of this approach to the study of a molecular motor system will be presented in forthcoming papers. The MS-LT-QFPE and MS-LT-QSE are also helpful for identifying purely quantum effects, because they allow us to compare the quantum results with the classical results obtained in the classical limit of the MS-LT-QFPE and MS-LT-QSE.

As shown in Appendix C, although the LT-QSE accurately predicts the quantum dynamics in the case of strong friction, while we must truncate the number of QLT correction terms properly with estimating the time scales of each term given by, ν_k, in comparison with the time scale of the system dynamics. A correction of the LT-QSE using conventional QSE theories may suppress this ambiguity. This is left for future investigations.

Because the (MS-)LT-QFPE is derived using a technique similar to that used in the conventional HEOM approach, an extension of the present formalism to the imaginary time formalism in calculations of the partition function should be straightforward.[32,78]

APPENDIX A: STOCHASTIC LIOUVILLE DESCRIPTION OF (MS-)LT-QFPE AND (MS-)LT-QSE

Because each contribution from the QLT terms is a Gaussian process, we can construct equations of motion in terms of continuous stochastic variables.[13,33] We introduce a set of stochastic variables $\vec{\Omega} \equiv (..., \Omega_k, ...)$, where Ω_k is the auxiliary stochastic variable for the description of the kth QLT correction term. Then, the Wigner distribution function is expressed as

$$\boldsymbol{W}^{d}(p, q, \vec{\Omega}, t) \equiv \sum_{\vec{n}} \boldsymbol{W}_{\vec{n}}^{d}(p, q, t)\phi_{\vec{n}}(\vec{\Omega}) \tag{50a}$$

The inverse relation is expressed as

$$\boldsymbol{W}_{\vec{n}}^{d}(p, q, t) = \int d\vec{\Omega}\boldsymbol{W}^{d}(p, q, \vec{\Omega}, t)\phi_{\vec{n}}^{(-1)}(\vec{\Omega}) \tag{50b}$$

Here, the functions $\phi_{\vec{n}}(\vec{\Omega})$ and $\phi_{\vec{n}}^{(-1)}(\vec{\Omega})$ are defined as

DOI: 10.1021/acs.jctc.8b01195
J. Chem. Theory Comput. 2019, 15, 2517−2534

$$\phi_{\vec{n}}(\vec{\Omega}) \equiv \frac{\prod_k^K b_k^{n_k}}{\sqrt{\prod_k^K n_k!}} \psi_{\vec{0}}(\vec{\Omega}) \psi_{\vec{n}}(\vec{\Omega}) \tag{51a}$$

and

$$\phi_{\vec{n}}^{(-1)}(\vec{\Omega}) \equiv \frac{\sqrt{\prod_k^K n_k!}}{\prod_k^K b_k^{n_k}} \psi_{\vec{n}}(\vec{\Omega}) \psi_{\vec{0}}(\vec{\Omega})^{-1} \tag{51b}$$

where $\psi_{\vec{n}}(\vec{\Omega})$ is the Hermite function, $\psi_{\vec{n}}(\vec{\Omega}) \equiv \prod_k^K \psi_{n_k}(\Omega_k)$, with

$$\psi_{n_k}(\Omega_k) \equiv \frac{1}{\sqrt{2^{n_k} n_k! \alpha_k \sqrt{\pi}}} H_{n_k}\left(\frac{\Omega_k}{\alpha_k}\right) \exp\left(-\frac{\Omega_k^2}{2\alpha_k^2}\right) \tag{52}$$

and the nth Hermite polynomial, $H_n(z) \equiv (-1)^n e^{z^2} (\partial^n / \partial z^n) e^{-z^2}$. The coefficients $\alpha_k \neq 0$ and $b_k \neq 0$ are real numbers. Then, the MS-WDF, $\boldsymbol{W}^{\mathrm{d}}(p, q, t) = \boldsymbol{W}_0^{\mathrm{d}}(p,q,t)$, can be expressed as

$$\boldsymbol{W}^{\mathrm{d}}(p, q, t) = \int \mathrm{d}\vec{\Omega} \boldsymbol{W}^{\mathrm{d}}(p, q, \vec{\Omega}, t) \tag{53}$$

because of the orthogonality of the Hermite functions.

While the coefficients α_k and b_k in eqs 51a and 51b can be chosen in an arbitrary manner, we found that the choice $\alpha_k = \sqrt{4\eta_k \zeta / \beta\hbar\omega_0 \nu_k}$ and $b_k = \sqrt{2/\alpha_k \nu_k}$ makes the equation of motion for $\boldsymbol{W}^{\mathrm{d}}(p, q, \vec{\Omega}, t)$ simple. Thus, we obtain the stochastic Liouville description of (MS)-LT-QFPE as

$$\frac{\partial}{\partial t} \boldsymbol{W}^{\mathrm{d}}(p, q, \vec{\Omega}, t) = -\left[\mathcal{L}_{\mathrm{qm}}(p, q) + \hat{\Xi}_K^{\mathrm{d}}(p, q) + \sum_k^K (\hat{\Phi}^{\mathrm{d}}(p, q) \hat{\Delta}_k(\Omega_k) + \hat{\Xi}_k^{(\nu)}(\Omega_k))\right] \boldsymbol{W}^{\mathrm{d}}(p, q, \vec{\Omega}, t) \tag{54}$$

where

$$\hat{\Delta}_k(\Omega_k) \equiv \nu_k \Omega_k + 2\frac{\zeta}{\omega_0} \frac{2\eta_k}{\beta\hbar} \frac{\partial}{\partial \Omega_k} \tag{55a}$$

and

$$\hat{\Xi}_k^{(\nu)}(\Omega_k) \equiv -\frac{\partial}{\partial \Omega_k}\left(\nu_k \Omega_k + \frac{\zeta}{\omega_0} \frac{2\eta_k}{\beta\hbar} \frac{\partial}{\partial \Omega_k}\right) \tag{55b}$$

For details of eq 54, see section S2. Note that, while eq 54 is similar to the Fokker–Planck equation for classical non-Markovian dynamics via Markovian-type Fokker–Planck equations with "virtual variables",[87,88] our variables $\vec{\Omega} = (..., \Omega_k, ...)$ are introduced to describe the QLT correction terms from the Bose–Einstein distribution function. Equation 50b is similar to the discretized representation of a phase-space distribution of the classical Kramer's equation (the Brinkman hierarchy).[19,63] Therefore, the (MS-)LT-QFPE can be regarded as the Brinkman hierarchy representation of eq 54.

Similarly, the (MS-)LT-QSE, eq 17, is equivalent to the equation of motion

$$\frac{\partial}{\partial t} \boldsymbol{f}^{\mathrm{d}}(q, \vec{\Omega}, t) = -\left[\mathcal{E}^{\mathrm{d}}(q) + \frac{\omega_0}{\zeta}(\mathcal{F}^{\mathrm{d}}(q) + \hat{\Xi}_K^{\mathrm{od,d}}(q)) + \sum_k^K (\hat{\Phi}^{\mathrm{od,d}}(q) \hat{\Delta}_k^{\mathrm{od}}(\Omega_k) + \hat{\Xi}_k^{(\nu)\mathrm{od}}(\Omega_k))\right] \boldsymbol{f}^{\mathrm{d}}(q, \vec{\Omega}, t) \tag{56}$$

where

$$\hat{\Delta}_k^{\mathrm{od}}(\Omega_k) \equiv \nu_k \Omega_k + 2\frac{\omega_0}{\zeta} \frac{2\eta_k}{\beta\hbar} \frac{\partial}{\partial \Omega_k} \tag{57a}$$

and

$$\hat{\Xi}_k^{(\nu)\mathrm{od}}(\Omega_k) \equiv -\frac{\partial}{\partial \Omega_k}\left(\nu_k \Omega_k + \frac{\omega_0}{\zeta} \frac{2\eta_k}{\beta\hbar} \frac{\partial}{\partial \Omega_k}\right) \tag{57b}$$

Further details of eq 56 are given in section S2.

APPENDIX B: LANGEVIN DESCRIPTIONS OF LT-QFPE AND LT-QSE

In the case that the system has only a single-state (i.e., in the case of that $\boldsymbol{W}^{\mathrm{d}}(p, q, t)$ and $\boldsymbol{U}^{\mathrm{d}}(q)$ reduce to scaler functions, $W(p, q, t)$ and $U(q)$) and the quantum nature of the nuclear dynamics is weak (i.e., anharmonicity of the potential is weak or friction is strong), higher-order terms of the Moyal product, eq 13, can be omitted and eq 12c is approximated as

$$\mathcal{U}_{\mathrm{qm}}(p, q) W(p, q) \simeq \mathcal{U}_{\mathrm{cl}}(p, q) W(p, q) \equiv F(q) \frac{\partial}{\partial p} W(p, q) \tag{58}$$

Here, we have introduced the force $F(q) \equiv -(1/\hbar)\partial U(q)/\partial q$. In a harmonic potential case, the above expression is exact. Then, eqs 11 and 54 can be decomposed into a set of Langevin equations

$$\dot{q}(t) = \omega_0 p(t) \tag{59a}$$

$$\dot{p}(t) = F(q(t)) - \zeta p(t) + \tilde{R}_q(t) + \sum_k^K \dot{\Omega}_k(t) \tag{59b}$$

and

$$\dot{\Omega}_k(t) = -\nu_k \Omega_k(t) + \tilde{R}_k^{(\nu)}(t) \tag{59c}$$

Here, $\Omega_k(t)$ is an auxiliary stochastic variable for the kth index of $\vec{n}$, and $\tilde{R}_q(t)$ and $\tilde{R}_k^{(\nu)}(t)$ are Gaussian-white forces that satisfy the relations

$$\langle \tilde{R}_q(t) \rangle = \langle \tilde{R}_k^{(\nu)}(t) \rangle = 0 \tag{60a}$$

$$\langle \tilde{R}_q(t) \tilde{R}_q(t') \rangle = \frac{\zeta}{\omega_0} \frac{1}{\beta\hbar} \cdot 2\delta(t - t') \tag{60b}$$

$$\langle \tilde{R}_k^{(\nu)}(t) \tilde{R}_k^{(\nu)}(t') \rangle = \frac{\zeta}{\omega_0} \frac{2\eta_k}{\beta\hbar} \cdot 2\delta(t - t') \tag{60c}$$

and $\langle \tilde{R}_q(t) \tilde{R}_k^{(\nu)}(t') \rangle = \langle \tilde{R}_k^{(\nu)}(t) \tilde{R}_k^{(\nu)}(t') \rangle = 0$ $(k \neq k')$. For details of eqs 59a–59c, see section S3. By introducing a quantum random force as

$$\tilde{R}_{\mathrm{qm}}(t) = \tilde{R}_q(t) + \sum_k^K \dot{\Omega}_k(t) \tag{61}$$

DOI: 10.1021/acs.jctc.8b01195
J. Chem. Theory Comput. 2019, 15, 2517–2534

the set of Langevin equations, eqs 59a, 59b, and 59c, can be rewritten as

$$\dot{q}(t) = \omega_0 p(t) \tag{62a}$$

and

$$\dot{p}(t) = F(q(t)) - \zeta p(t) + \tilde{R}_{\mathrm{qm}}(t) \tag{62b}$$

The random force $\tilde{R}_{\mathrm{qm}}(t)$ satisfies the QFD theorem as

$$\langle \tilde{R}_{\mathrm{qm}}(t)\tilde{R}_{\mathrm{qm}}(t')\rangle = C_K(t-t') \tag{63a}$$

$$\xrightarrow[K\to\infty]{} 2\int \mathrm{d}\omega \frac{\zeta}{\omega_0}\omega\left(n(\omega)+\frac{1}{2}\right)\cos\omega(t-t') \tag{63b}$$

The set of eqs 62a and 62b are the quantum Langevin equation[10,57] for the c-number variables, $p(t)$ and $q(t)$ (i.e., the quasi-classical Langevin equation[89,90]). In the cases that anharmonicity of the system is strong, we cannot employ the above equations. In such cases, we have to evaluate the quantum Langevin equation described by the operators, $\hat{p}(t)$ and $\hat{q}(t)$, or to employ Wigner description (i.e., eqs 11 and 54) with the quantum Liouvillian (eq 12a). This indicates that, the LT-QFPE, eqs 11 and 54, can be regarded as the Fokker–Planck equations equivalent to the quantum Langevin equation. Note that, while eqs 59a, 59b, and 59c are similar to the generalized Langevin equation for classical non-Markovian dynamics via Markovian-type Lanvegin equations with virtual variables,[87,88,91,92] our stochastic variables $\vec{\Omega} = (..., \omega_k, ...)$ are introduced to describe the QLT correction terms from the Bose–Einstein distribution function.

It should be noted that, for the LT-QFPE with a single PES, eq 17 can also be decomposed into a set of Langevin equations

$$\frac{\zeta}{\omega_0}\dot{q}(t) = F(q(t)) + \tilde{R}_q(t) + \sum_k^K \dot{\Omega}_k(t) \tag{64a}$$

and

$$\dot{\Omega}_k(t) = -\nu_k\Omega_k + \tilde{R}_k^{(\nu)}(t) \tag{64b}$$

By introducing $\tilde{R}_{\mathrm{qm}}(t)$, the set of Langevin equations, eqs 64a and 64b, can be rewritten as

$$\frac{\zeta}{\omega_0}\dot{q}(t) = F(q(t)) + \tilde{R}_{\mathrm{qm}}(t) \tag{65}$$

This is the "overdamped" quantum Langevin equation for the c-number variable, $q(t)$ (i.e., the inertia term $\propto\ddot{q}(t)$ is omitted). For details of eqs 64a and 64b, see section S3.

APPENDIX C: COMPARISON OF QSE AND LT-QSE

In this appendix, we compare our LT-QSE theory with conventional QSE theories.

The QSE is proposed in refs 48, 49, and 65. It is given by

$$\frac{\partial}{\partial t}f(q,t) = \frac{\omega_0}{\zeta}\frac{\partial}{\partial q}\left[\frac{1}{\hbar}\frac{\partial U(q)}{\partial q} + \frac{1}{\beta\hbar}\left(1+\beta\lambda\frac{\partial^2 U(q)}{\partial q^2}\right)\frac{\partial}{\partial q}\right]f(q,t) \tag{66}$$

in terms of our dimensionless coordinate q. Here, we have

$$\lambda \equiv \frac{\omega_0}{\pi\zeta}\log\left(\frac{\beta\hbar\zeta}{2\pi}\right) \tag{67}$$

In the case of the harmonic oscillator (eq 20), eq 66 can be written

$$\frac{\partial}{\partial t}f(q,t) = \frac{{\omega_0}^2}{\zeta}\frac{\partial}{\partial q}\left[q + \frac{1}{\beta\hbar\omega_0}(1+\beta\hbar\omega_0\lambda)\frac{\partial}{\partial q}\right]f(q,t) \tag{68}$$

Better quantum corrections for the QSE are presented in refs 66 and 67. For a harmonic potential, this becomes

$$\frac{\partial}{\partial t}f(q,t) = \Omega\frac{\partial}{\partial q}\left(q + \langle q^2\rangle_{\beta,\zeta}\frac{\partial}{\partial q}\right)f(q,t) \tag{69}$$

where $\Omega \equiv \zeta/2 - \sqrt{(\zeta/2)^2 - {\omega_0}^2}$ and $\langle q^2\rangle_{\beta,\zeta}$ is given in eq 22b. Hereafter, we refer to eqs 68 and 69 as the QSE and QSE′, respectively.

In Figure 8, we display the steady-state solutions of the QSE, QSE′, and LT-QSE for several values of the damping strength

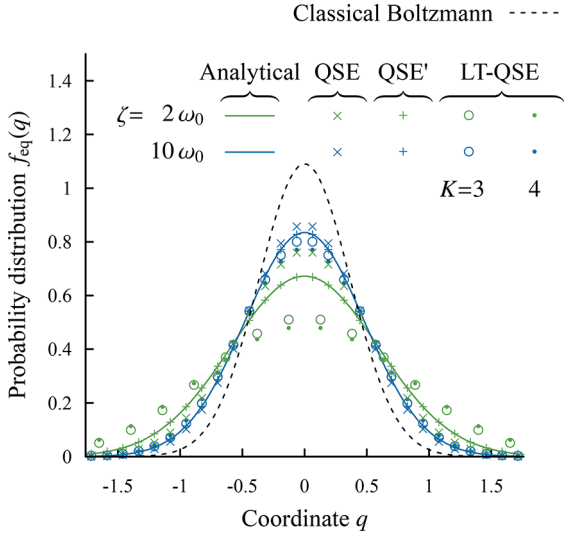

Figure 8. Equilibrium distribution, $f_{\mathrm{eq}}(q)$, calculated with the QSE, QSE′, and LT-QSE for the critically damped, $\zeta = 2\omega_0$ (green), and overdamped, $\zeta = 10\omega_0$ (blue), cases at low temperature, $\beta\hbar\omega_0 = 7.47$. The classical (dashed) and quantum (solid) equilibrium distributions were obtained from the analytical expression in eq 21.

at low temperature, $\beta\hbar\omega_0 = 7.47$. The other parameter values are the same as in section 3.1. In the overdamped case, all calculated results are qualitatively similar to the analytical result. This is because the QSE and QSE′ are constructed so as to reproduce the steady-state solution. The QSE′, in particular, utilizes $\langle q^2\rangle_{\beta,\zeta}$; for this reason, it reproduces the analytical result even in the critical-damping case.

Note that if we assume the overdamped approximation eq 28 for the analytical equilibrium distribution eq 21 instead of eq 23, the integral in eq 22b diverges under the infinite summation of the Matsubara frequencies as

$$\langle q^2\rangle_{\beta,\zeta}^{\zeta\gg\omega_0} = \frac{\tilde{\gamma}}{\beta\hbar\omega_0}\sum_{k=-\infty}^{\infty}\frac{1}{\tilde{\gamma}+|\tilde{\nu}_k|} \to \infty \tag{70}$$

The calculated results using the LT-QSE theory become close to the above analytical result by employing larger hierarchical space (i.e., by increasing K). Thus, the steady-state solution predicted by the LT-QSE theory deviates as K increases. This divergence is similar to the ultraviolet divergence of $\langle p^2\rangle$. This indicates that, in order to calculate physical quantities on the basis of LT-QSE, we must truncate the number of QLT

DOI: 10.1021/acs.jctc.8b01195
J. Chem. Theory Comput. 2019, 15, 2517−2534

correction terms properly by estimating the time scales of them, ν_k, in comparison with the time scale of the system dynamics. Note that a Drude spectral density model for reduced electronic states has also this problem because eq 28 is equivalent to the symmetrized correlation function of the collective noise coordinate in the Drude spectral density model.

In Figure 9, we display the symmetrized correlation functions calculated with the QSE, QSE′, and LT-QSE

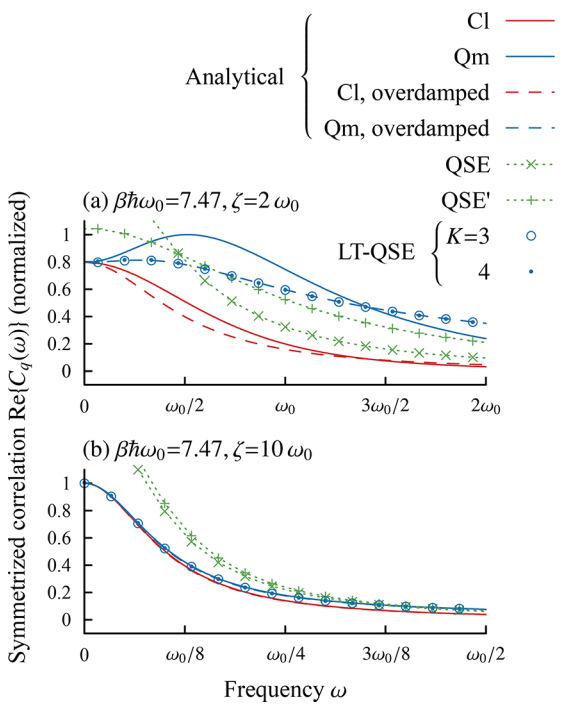

Figure 9. Symmetrized correlation functions, $C(\omega)$, calculated with the QSE, QSE′, and LT-QSE for the (a) critically damped and (b) overdamped cases at low temperature, $\beta\hbar\omega_0 = 7.47$. The solid and dashed curves represent the analytically derived solution, eq 23, and its overdamped limit, eq 28, respectively. The red and blue curves were obtained with classical and quantum treatments of $\coth(\beta\hbar\omega/2)$. The values are normalized with respect to the maximum of eq 23.

under the same conditions as in the case of Figure 8. Because the QSE and QSE′ attempt to account for all quantum corrections with Markovian terms ignoring the non-Markovian nature of the quantum noise, they cannot reproduce the dynamics at low temperature. In contrast, the calculated results with the LT-QSE theory become close to the exact solution in the overdamped case, eq 23, by increasing K, and both numerical results and eq 23 approach the solution eq 28 for large ζ.

APPENDIX D: ZUSMAN EQUATION

In this appendix, we show the relation between the present equation and Zusman equation. For simplicity, we assume a two-level system described by the diabatic harmonic PESs as

$$\boldsymbol{U}^{\mathrm{d}}(q) = \boldsymbol{A} - \hbar d\omega_0 \boldsymbol{B} q + \frac{\hbar\omega_0}{2} q^2 \tag{71a}$$

and

$$\boldsymbol{F}^{\mathrm{d}}(q) = -\frac{1}{\hbar}\frac{\partial \boldsymbol{U}^{\mathrm{d}}(q)}{\partial q} = d\omega_0 \boldsymbol{B} - \omega_0 q \tag{71b}$$

with matrices

$$\boldsymbol{A} = \begin{pmatrix} 0 & V \\ V & E_0 \end{pmatrix} \text{ and } \boldsymbol{B} = \begin{pmatrix} 0 & 0 \\ 0 & 1 \end{pmatrix} \tag{72}$$

Here, V is the diabatic coupling constant between $|0\rangle$ and $|1\rangle$, d is the dimensionless displacement between the minima of two PESs, and $E_0 \equiv \Delta E + \lambda$ is the summation of the driving force ΔE and the reorganization energy $\lambda \equiv \hbar\omega_0 d^2/2$. In this case, the MS-SE can be rewritten as

$$\frac{\partial}{\partial t}\boldsymbol{f}^{\mathrm{d}}(q,t) = -\frac{i}{\hbar}\boldsymbol{A}^{\times}\boldsymbol{f}^{\mathrm{d}}(q,t) + d\omega_0 q i\boldsymbol{B}^{\times}\boldsymbol{f}^{\mathrm{d}}(q,t) - \tilde{\gamma} d\frac{\partial}{\partial q}\frac{1}{2}\boldsymbol{B}^{\circ}\boldsymbol{f}^{\mathrm{d}}(q,t) + \hat{\Gamma}(q)\boldsymbol{f}^{\mathrm{d}}(q,t) \tag{73}$$

Here, we have introduced commutation and anticommutation hyper operators, $\boldsymbol{O}^{\times/\circ}\boldsymbol{f} \equiv \boldsymbol{O}\boldsymbol{f} \mp \boldsymbol{f}\boldsymbol{O}$, and

$$\hat{\Gamma}(q) \equiv \tilde{\gamma}\frac{\partial}{\partial q}\left(q + \frac{1}{\beta\hbar\omega_0}\frac{\partial}{\partial q}\right) \tag{74}$$

Note that eq 73 is equivalent to the stochastic Liouville representation of the HEOM for a Drude spectral density in the high-temperature limit, given in refs 33 and 51. When we neglect the electronic−nuclear interaction from the force term (i.e., $\boldsymbol{F}^{\mathrm{d}}(q) \to -\omega_0 q$ and the anticommutation term ($\propto \boldsymbol{B}^{\circ}$) is omitted from eq 73), we obtain the ZE in a matrix representation as

$$\frac{\partial}{\partial t}\boldsymbol{f}^{\mathrm{d}}(q,t) = -\frac{i}{\hbar}\boldsymbol{A}^{\times}\boldsymbol{f}^{\mathrm{d}}(q,t) + d\omega_0 q i\boldsymbol{B}^{\times}\boldsymbol{f}^{\mathrm{d}}(q,t) + \hat{\Gamma}(q)\boldsymbol{f}^{\mathrm{d}}(q,t) \tag{75}$$

The equations of motion for diabatic matrix elements are expressed as

$$\frac{\partial}{\partial t}f_{00}^{\mathrm{d}}(q,t) = -\frac{i}{\hbar}(f_{10}^{\mathrm{d}}(q,t) - f_{01}^{\mathrm{d}}(q,t))V + \hat{\Gamma}(q)f_{00}^{\mathrm{d}}(q,t) \tag{76a}$$

$$\frac{\partial}{\partial t}f_{11}^{\mathrm{d}}(q,t) = -\frac{i}{\hbar}(f_{01}^{\mathrm{d}}(q,t) - f_{10}^{\mathrm{d}}(q,t))V + \hat{\Gamma}(q)f_{11}^{\mathrm{d}}(q,t) \tag{76b}$$

and

$$\frac{\partial}{\partial t}f_{01}^{\mathrm{d}}(q,t) = -\frac{i}{\hbar}f_{01}^{\mathrm{d}}(q,t)(\hbar\omega_0 dq - E_0) - \frac{i}{\hbar}(f_{11}^{\mathrm{d}}(q,t) - f_{00}^{\mathrm{d}}(q,t))V + \hat{\Gamma}(q)f_{01}^{\mathrm{d}}(q,t) \tag{76c}$$

The above equations are equivalent to the original ZE in ref 50 except the shift and scaling factors of q. As this derivation indicates, the MS-SE can be regarded as a generalization of the ZE for arbitrary PESs with including the quantum dynamical effects arising from the electric states. Note that the ZE for harmonic PESs including this dynamical effect is given in refs 38 and 51. This is also sometimes referred to as the ZE.

APPENDIX E: ADIABATIC REPRESENTATIONS OF MS-LT-QFPE AND MS-LT-QSE

In this appendix, we present the adiabatic representations of MS-LT-QFPE (eq 11) and MS-LT-QSE (eq 17).

DOI: 10.1021/acs.jctc.8b01195
J. Chem. Theory Comput. 2019, 15, 2517−2534

We can rewrite eqs 36 and 37 in terms of the Moyal star product, eq 13, as

$$\boldsymbol{W}^{\mathrm{a}}(p, q, t) = \boldsymbol{Z}(q)^{\dagger} \bigstar \boldsymbol{W}^{\mathrm{d}}(p, q, t) \bigstar \boldsymbol{Z}(q) \tag{77}$$

Inserting this into eq 11, we obtain the MS-QFP-LT in the adiabatic representation as

$$\begin{aligned}\frac{\partial}{\partial t}\boldsymbol{W}^{\mathrm{a}}_{\vec{n}}(p, q, t) &= -\left(\mathcal{L}^{\mathrm{a}}_{\mathrm{qm}}(p, q) + \sum_k^K n_k\gamma_k + \hat{\Xi}^{\mathrm{a}}_{\mathrm{qm}}(p, q)\right)\boldsymbol{W}^{\mathrm{a}}_{\vec{n}}(p, q, t) \\ &\quad - \sum_k^K \hat{\Phi}^{\mathrm{a}}(p, q)\boldsymbol{W}^{\mathrm{a}}_{\vec{n}+\vec{e}_k}(p, q, t) \\ &\quad - \sum_k^K n_k\gamma_k\hat{\Theta}^{\mathrm{a}}_k(p, q)\boldsymbol{W}^{\mathrm{a}}_{\vec{n}-\vec{e}_k}(p, q, t)\end{aligned} \tag{78}$$

where

$$\mathcal{L}^{\mathrm{a}}_{\mathrm{qm}}(p, q) \equiv \mathcal{K}(p, q) + \mathcal{U}^{\mathrm{a}}_{\mathrm{qm}}(p, q) + \mathcal{D}^{\mathrm{a}}_{\mathrm{qm}}(p, q) \tag{79a}$$

is the quantum Liouvillian for the MSWDF in the adiabatic representation, and we have

$$\mathcal{U}^{\mathrm{a}}_{\mathrm{qm}}(p, q)\boldsymbol{W}^{\mathrm{a}}(p, q) \equiv \frac{i}{\hbar}\boldsymbol{U}^{\mathrm{a}}(q)^{\times_{(\star)}}\boldsymbol{W}^{\mathrm{a}}(p, q) \tag{79b}$$

and

$$\begin{aligned}&\mathcal{D}_{\mathrm{qm}}(p, q)\boldsymbol{W}^{\mathrm{a}}(p, q) \\ &\equiv -i\frac{\omega_0}{2}\boldsymbol{d}(q)^{\circ_{(\star)}}\frac{\partial \boldsymbol{W}^{\mathrm{a}}(p, q)}{\partial q} + \omega_0\boldsymbol{d}(q)^{\times_{(\star)}}p\boldsymbol{W}^{\mathrm{a}}(p, q) \\ &\quad - \frac{i\omega_0}{2}(\boldsymbol{h}(q)\bigstar\boldsymbol{W}^{\mathrm{a}}(p, q) - \boldsymbol{W}^{\mathrm{a}}(p, q)\bigstar\boldsymbol{h}(q)^{\dagger})\end{aligned} \tag{79c}$$

Here, we have introduced the commutation and anticommutation hyper operators with the Moyal product, $\boldsymbol{O}^{\times/\circ_{(\star)}}\boldsymbol{f} \equiv \boldsymbol{O}\bigstar\boldsymbol{f} \mp \boldsymbol{f}\bigstar\boldsymbol{O}$. The non-Markovian noise terms are $\hat{\Phi}^{\mathrm{a}}(p, q) \equiv \hat{\Phi}^{\mathrm{d}}(p, q)$ and $\hat{\Theta}^{\mathrm{a}}_k(p, q) \equiv \hat{\Theta}^{\mathrm{d}}_k(p,q)$, and the Markovian noise term, eq 15c, becomes

$$\begin{aligned}&\hat{\Xi}^{\mathrm{a}}_{\mathrm{qm}}(p, q)\boldsymbol{W}^{\mathrm{a}}(p, q) \\ &\equiv -\frac{\zeta}{\omega_0}\frac{\partial}{\partial p}\left(\omega_0 p\boldsymbol{W}^{\mathrm{a}}(p, q) - \frac{i\omega_0}{2}\boldsymbol{d}(p, q)^{\circ_{(\star)}}\boldsymbol{W}^{\mathrm{a}}(p, q)\right. \\ &\quad \left. + \frac{1}{\beta\hbar}\frac{\partial}{\partial p}\boldsymbol{W}^{\mathrm{a}}(p, q)\right) + \sum_k^K \hat{\Phi}^{\mathrm{a}}(p, q)\hat{\Theta}^{\mathrm{a}}_k(p, q)\boldsymbol{W}^{\mathrm{a}}(p, q)\end{aligned} \tag{80}$$

In the Smoluchowski limit, we introduce the adiabatic representation of $\boldsymbol{f}^{\mathrm{d}}(q)$

$$\boldsymbol{f}^{\mathrm{a}}(q, t) = \boldsymbol{Z}(q)^{\dagger}\boldsymbol{f}^{\mathrm{d}}(q, t)\boldsymbol{Z}(q) \tag{81}$$

Here, we have omitted the higher-order contributions from the Moyal product in eq 77 because such contributions from the quantum coherence, $z-z'$, have been removed in the Smoluchowski limit. Then the MS-LT-QSE (eq 17) becomes

$$\begin{aligned}\frac{\partial}{\partial t}\boldsymbol{f}^{\mathrm{a}}_{\vec{n}}(q, t) &= -\left[\mathcal{E}^{\mathrm{a}}(q) + \sum_k^K n_k\gamma_k + \frac{\omega_0}{\zeta}(\mathcal{F}^{\mathrm{a}}(q) + \hat{\Xi}^{\mathrm{od,a}}_K(q))\right]\boldsymbol{f}^{\mathrm{a}}_{\vec{n}}(q, t) \\ &\quad - \sum_k^K \hat{\Phi}^{\mathrm{od,a}}(q)\boldsymbol{f}^{\mathrm{a}}_{\vec{n}+\vec{e}_k}(q, t) \\ &\quad - \frac{\omega_0}{\zeta}\sum_k^K n_k\gamma_k\hat{\Theta}^{\mathrm{od,a}}_k(q)\boldsymbol{f}^{\mathrm{a}}_{\vec{n}-\vec{e}_k}(q, t)\end{aligned} \tag{82}$$

where the operators appearing in eq 17 are transformed as

$$\mathcal{E}^{\mathrm{a}}(q)\boldsymbol{f}(q) \equiv \frac{i}{\hbar}\boldsymbol{U}^{\mathrm{a}}(q)^{\times}\boldsymbol{f}(q) \tag{83a}$$

$$\begin{aligned}\mathcal{F}^{\mathrm{a}}(q)\boldsymbol{f}^{\mathrm{a}}(q) &\equiv \frac{1}{2}\boldsymbol{F}^{\mathrm{a}}(q)^{\circ}\left(\frac{\partial}{\partial q} + \boldsymbol{d}(q)^{\times}\right)\boldsymbol{f}^{\mathrm{a}}(q) \\ &\quad + \frac{1}{2\hbar}\boldsymbol{A}^{\mathrm{a}}(q)^{\circ}\boldsymbol{f}^{\mathrm{a}}(q)\end{aligned} \tag{83b}$$

$$\hat{\Phi}^{\mathrm{od,a}}(q)\boldsymbol{f}^{\mathrm{a}}(q) \equiv -\left(\frac{\partial}{\partial q} + \boldsymbol{d}(q)^{\times}\right)\boldsymbol{f}^{\mathrm{a}}(q) \tag{84a}$$

$$\hat{\Theta}^{\mathrm{od,a}}_k(q)\boldsymbol{f}^{\mathrm{a}}(q) \equiv \frac{2\eta_k}{\beta\hbar}\left(\frac{\partial}{\partial q} + \boldsymbol{d}(q)^{\times}\right)\boldsymbol{f}^{\mathrm{a}}(q) \tag{84b}$$

and

$$\begin{aligned}\hat{\Xi}^{\mathrm{od,a}}_K(q)\boldsymbol{f}^{\mathrm{a}}(q) &\equiv -\frac{1}{\beta\hbar}\left(\frac{\partial}{\partial q} + \boldsymbol{d}(q)^{\times}\right)^2\boldsymbol{f}^{\mathrm{a}}(q) \\ &\quad + \sum_k^K \hat{\Phi}^{\mathrm{a}}(q)\hat{\Theta}^{\mathrm{a}}_k(q)\end{aligned} \tag{84c}$$

Here, we have introduced the force acting on the adiabatic states

$$\begin{aligned}\boldsymbol{F}^{\mathrm{a}}(q) &\equiv \boldsymbol{Z}(q)^{\dagger}\boldsymbol{F}^{\mathrm{d}}(q)\boldsymbol{Z}(q) \\ &= -\frac{1}{\hbar}\frac{\partial \boldsymbol{U}^{\mathrm{a}}(q)}{\partial q} - \frac{1}{\hbar}(\boldsymbol{d}(q)\boldsymbol{U}^{\mathrm{a}}(q) - \boldsymbol{U}^{\mathrm{a}}(q)\boldsymbol{d}(q))\end{aligned} \tag{85}$$

and its derivative

$$\begin{aligned}\boldsymbol{A}^{\mathrm{a}}(q) &\equiv \boldsymbol{Z}(q)^{\dagger}\frac{\partial \boldsymbol{F}^{\mathrm{d}}(q)}{\partial q}\boldsymbol{Z}(q) \\ &= \frac{\partial \boldsymbol{F}^{\mathrm{a}}(q)}{\partial q} - \boldsymbol{d}(q)\boldsymbol{F}^{\mathrm{a}}(q) + \boldsymbol{F}^{\mathrm{a}}\boldsymbol{d}(q)\end{aligned} \tag{86}$$

■ ASSOCIATED CONTENT

Supporting Information

The Supporting Information is available free of charge on the ACS Publications website at DOI: 10.1021/acs.jctc.8b01195.

C++ source codes that we developed, which allow for the treatment of the phase and coordinate space dynamics with any single-state or multistate potential forms (ZIP)

Derivations of the (MS-)LT-QFPE and (MS-)LT-QSE, derivation of the stochastic Liouville and Langevin descriptions of (MS-)LT-QFPE and (MS-)LT-QSE, truncation scheme of hierarchy, note on the ultraviolet divergence, and details of the numerical calculations (PDF)

■ AUTHOR INFORMATION

Corresponding Authors

*E-mail: ikeda.tatsushi.37u@kyoto-u.jp.

*E-mail: tanimura.yoshitaka.5w@kyoto-u.jp.

ORCID

Yoshitaka Tanimura: 0000-0002-7913-054X

Notes

The authors declare no competing financial interest.

■ ACKNOWLEDGMENTS

This work was supported by JSPS KAKENHI Grant Number JP26248005.

REFERENCES

(1) Polli, D.; Altoé, P.; Weingart, O.; Spillane, K. M.; Manzoni, C.; Brida, D.; Tomasello, G.; Orlandi, G.; Kukura, P.; Mathies, R. A.; Garavelli, M.; Cerullo, G. Conical intersection dynamics of the primary photoisomerization event in vision. *Nature* **2010**, *467*, 440.

(2) Iwamura, M.; Watanabe, H.; Ishii, K.; Takeuchi, S.; Tahara, T. Coherent Nuclear Dynamics in Ultrafast Photoinduced Structural Change of Bis(diimine)copper(I) Complex. *J. Am. Chem. Soc.* **2011**, *133*, 7728.

(3) Lewis, N. H. C.; Fleming, G. R. Two-Dimensional Electronic-Vibrational Spectroscopy of Chlorophyll a and b. *J. Phys. Chem. Lett.* **2016**, *7*, 831.

(4) Dean, J. C.; Mirkovic, T.; Toa, Z. S. D.; Oblinsky, D. G.; Scholes, G. D. Vibronic Enhancement of Algae Light Harvesting. *Chem.* **2016**, *1*, 858.

(5) Miyata, K.; Kurashige, Y.; Watanabe, K.; Sugimoto, T.; Takahashi, S.; Tanaka, S.; Takeya, J.; Yanai, T.; Matsumoto, Y. Coherent singlet fission activated by symmetry breaking. *Nat. Chem.* **2017**, *9*, 983.

(6) Prokhorenko, V. I.; Picchiotti, A.; Pola, M.; Dijkstra, A. G.; Miller, R. J. D. New Insights into the Photophysics of DNA Nucleobases. *J. Phys. Chem. Lett.* **2016**, *7*, 4445.

(7) Kato, A.; Ishizaki, A. Non-Markovian Quantum-Classical Ratchet for Ultrafast Long-Range Electron-Hole Separation in Condensed Phases. *Phys. Rev. Lett.* **2018**, *121*, 026001.

(8) Dümcke, R.; Spohn, H. The proper form of the generator in the weak coupling limit. *Z. Phys. B: Condens. Matter Quanta* **1979**, *34*, 419−422.

(9) Pechukas, P. Reduced Dynamics Need Not Be Completely Positive. *Phys. Rev. Lett.* **1994**, *73*, 1060−1062.

(10) Ford, G. W.; Lewis, J. T.; O'Connell, R. F. Quantum Langevin equation. *Phys. Rev. A: At., Mol., Opt. Phys.* **1988**, *37*, 4419−4428.

(11) Frantsuzov, P. A. The failure of the diffusional description of the level crossing problem I. Violation of the von Neumann conditions. *Chem. Phys. Lett.* **1997**, *267*, 427−430.

(12) Dammak, H.; Chalopin, Y.; Laroche, M.; Hayoun, M.; Greffet, J.-J. Quantum Thermal Bath for Molecular Dynamics Simulation. *Phys. Rev. Lett.* **2009**, *103*, 190601.

(13) Tanimura, Y. Stochastic Liouville, Langevin, Fokker-Planck, and Master Equation Approaches to Quantum Dissipative Systems. *J. Phys. Soc. Jpn.* **2006**, *75*, 082001.

(14) Thoss, M.; Miller, W. H.; Stock, G. Semiclassical description of nonadiabatic quantum dynamics: Application to the S1-S2 conical intersection in pyrazine. *J. Chem. Phys.* **2000**, *112*, 10282.

(15) Kühl, A.; Domcke, W. Multilevel Redfield description of the dissipative dynamics at conical intersections. *J. Chem. Phys.* **2002**, *116*, 263.

(16) Tanimura, Y.; Mukamel, S. Multistate quantum Fokker-Planck approach to nonadiabatic wave packet dynamics in pump-probe spectroscopy. *J. Chem. Phys.* **1994**, *101*, 3049−3061.

(17) Tanimura, Y.; Maruyama, Y. Gaussian-Markovian quantum Fokker-Planck approach to nonlinear spectroscopy of a displaced Morse potentials system: Dissociation, predissociation, and optical Stark effects. *J. Chem. Phys.* **1997**, *107*, 1779.

(18) Maruyama, Y.; Tanimura, Y. Pump-probe spectra and nuclear dynamics for a dissipative molecular system in a strong laser field: predissociation dynamics. *Chem. Phys. Lett.* **1998**, *292*, 28.

(19) Ikeda, T.; Tanimura, Y. Probing photoisomerization processes by means of multi-dimensional electronic spectroscopy: The multi-state quantum hierarchical Fokker-Planck equation approach. *J. Chem. Phys.* **2017**, *147*, 014102.

(20) Ikeda, T.; Tanimura, Y. Phase-space wavepacket dynamics of internal conversion via conical intersection: Multi-state quantum Fokker-Planck equation approach. *Chem. Phys.* **2018**, *515*, 203−213.

(21) Kapral, R.; Ciccotti, G. Mixed quantum-classical dynamics. *J. Chem. Phys.* **1999**, *110*, 8919.

(22) Xie, W.; Xu, Y.; Zhu, L.; Shi, Q. Mixed quantum classical calculation of proton transfer reaction rates: From deep tunneling to over the barrier regimes. *J. Chem. Phys.* **2014**, *140*, 174105.

(23) Ben-Nun, M.; Martínez, T. J. Nonadiabatic molecular dynamics: Validation of the multiple spawning method for a multidimensional problem. *J. Chem. Phys.* **1998**, *108*, 7244.

(24) Ben-Nun, M.; Quenneville, J.; Martínez, T. J. Ab Initio Multiple Spawning: Photochemistry from First Principles Quantum Molecular Dynamics. *J. Phys. Chem. A* **2000**, *104*, 5161.

(25) Makhov, D. V.; Glover, W. J.; Martínez, T. J.; Shalashilin, D. V. Ab initio multiple cloning algorithm for quantum nonadiabatic molecular dynamics. *J. Chem. Phys.* **2014**, *141*, 054110.

(26) Tully, J. C. Molecular dynamics with electronic transitions. *J. Chem. Phys.* **1990**, *93*, 1061.

(27) Coker, D. F.; Xiao, L. Methods for molecular dynamics with nonadiabatic transitions. *J. Chem. Phys.* **1995**, *102*, 496.

(28) Subotnik, J. E.; Jain, A.; Landry, B.; Petit, A.; Ouyang, W.; Bellonzi, N. Understanding the Surface Hopping View of Electronic Transitions and Decoherence. *Annu. Rev. Phys. Chem.* **2016**, *67*, 387.

(29) Caldeira, A. O.; Leggett, A. J. Path integral approach to quantum Brownian motion. *Phys. A* **1983**, *121*, 587.

(30) Tanimura, Y.; Wolynes, P. G. Quantum and classical Fokker-Planck equations for a Gaussian-Markovian noise bath. *Phys. Rev. A: At., Mol., Opt. Phys.* **1991**, *43*, 4131.

(31) Tanimura, Y.; Wolynes, P. G. The interplay of tunneling, resonance, and dissipation in quantum barrier crossing: A numerical study. *J. Chem. Phys.* **1992**, *96*, 8485−8496.

(32) Tanimura, Y. Real-time and imaginary-time quantum hierarchal Fokker-Planck equations. *J. Chem. Phys.* **2015**, *142*, 144110.

(33) Tanimura, Y.; Kubo, R. Time Evolution of a Quantum System in Contact with a Nearly Gaussian-Markoffian Noise Bath. *J. Phys. Soc. Jpn.* **1989**, *58*, 101.

(34) Ishizaki, A.; Tanimura, Y. Quantum Dynamics of System Strongly Coupled to Low-Temperature Colored Noise Bath: Reduced Hierarchy Equations Approach. *J. Phys. Soc. Jpn.* **2005**, *74*, 3131.

(35) Ishizaki, A.; Fleming, G. R. Unified treatment of quantum coherent and incoherent hopping dynamics in electronic energy transfer: Reduced hierarchy equation approach. *J. Chem. Phys.* **2009**, *130*, 234111.

(36) Fujihashi, Y.; Fleming, G. R.; Ishizaki, A. Impact of environmentally induced fluctuations on quantum mechanically mixed electronic and vibrational pigment states in photosynthetic energy transfer and 2D electronic spectra. *J. Chem. Phys.* **2015**, *142*, 212403.

(37) Leggett, A. J. Quantum tunneling in the presence of an arbitrary linear dissipation mechanism. *Phys. Rev. B: Condens. Matter Mater. Phys.* **1984**, *30*, 1208−1218.

(38) Garg, A.; Onuchic, J. N.; Ambegaokar, V. Effect of friction on electron transfer in biomolecules. *J. Chem. Phys.* **1985**, *83*, 4491−4503.

(39) Tanimura, Y.; Mukamel, S. Optical Stark Spectroscopy of a Brownian Oscillator in Intense Fields. *J. Phys. Soc. Jpn.* **1994**, *63*, 66−77.

(40) Tanimura, Y. Reduced hierarchy equations of motion approach with Drude plus Brownian spectral distribution: Probing electron transfer processes by means of two-dimensional correlation spectroscopy. *J. Chem. Phys.* **2012**, *137*, 22A550.

(41) Ishizaki, A.; Tanimura, Y. Modeling vibrational dephasing and energy relaxation of intramolecular anharmonic modes for multi-dimensional infrared spectroscopies. *J. Chem. Phys.* **2006**, *125*, 084501.

(42) Sakurai, A.; Tanimura, Y. Does $\hbar$ Play a Role in Multidimensional Spectroscopy? Reduced Hierarchy Equations of Motion Approach to Molecular Vibrations. *J. Phys. Chem. A* **2011**, *115*, 4009.

(43) Ikeda, T.; Ito, H.; Tanimura, Y. Analysis of 2D THz-Raman spectroscopy using a non-Markovian Brownian oscillator model with nonlinear system-bath interactions. *J. Chem. Phys.* **2015**, *142*, 212421.

(44) Kato, A.; Tanimura, Y. Quantum Suppression of Ratchet Rectification in a Brownian System Driven by a Biharmonic Force. *J. Phys. Chem. B* **2013**, *117*, 13132.

DOI: 10.1021/acs.jctc.8b01195
J. Chem. Theory Comput. 2019, 15, 2517−2534

(45) Sakurai, A.; Tanimura, Y. An Approach to Quantum Transport Based on Reduced Hierarchy Equations of Motion: Application to a Resonant Tunneling Diode. *J. Phys. Soc. Jpn.* **2013**, *82*, 033707.
(46) Sakurai, A.; Tanimura, Y. Self-excited current oscillations in a resonant tunneling diode described by a model based on the Caldeira-Leggett Hamiltonian. *New J. Phys.* **2014**, *16*, 015002.
(47) Grabert, H.; Schramm, P.; Ingold, G.-L. Quantum Brownian motion: The functional integral approach. *Phys. Rep.* **1988**, *168*, 115−207.
(48) Pechukas, P.; Ankerhold, J.; Grabert, H. Quantum Smoluchowski equation. *Ann. Phys. (Berlin, Ger.)* **2000**, *9*, 794.
(49) Ankerhold, J.; Pechukas, P.; Grabert, H. Strong Friction Limit in Quantum Mechanics: The Quantum Smoluchowski Equation. *Phys. Rev. Lett.* **2001**, *87*, 086802.
(50) Zusman, L. D. Outer-sphere electron transfer in polar solvents. *Chem. Phys.* **1980**, *49*, 295.
(51) Shi, Q.; Chen, L.; Nan, G.; Xu, R.-X.; Yan, Y. Electron transfer dynamics: Zusman equation versus exact theory. *J. Chem. Phys.* **2009**, *130*, 164518.
(52) Shi, Q.; Geva, E. A self-consistent treatment of electron transfer in the limit of strong friction via the mixed quantum classical Liouville method. *J. Chem. Phys.* **2009**, *131*, 034511.
(53) Tanimura, Y. Nonperturbative expansion method for a quantum system coupled to a harmonic-oscillator bath. *Phys. Rev. A: At., Mol., Opt. Phys.* **1990**, *41*, 6676−6687.
(54) Hu, J.; Xu, R.-X.; Yan, Y. Communication: Pad'e spectrum decomposition of Fermi function and Bose function. *J. Chem. Phys.* **2010**, *133*, 101106.
(55) Hu, J.; Luo, M.; Jiang, F.; Xu, R.-X.; Yan, Y. Padé spectrum decompositions of quantum distribution functions and optimal hierarchical equations of motion construction for quantum open systems. *J. Chem. Phys.* **2011**, *134*, 244106.
(56) Ding, J.-J.; Xu, R.-X.; Yan, Y. Optimizing hierarchical equations of motion for quantum dissipation and quantifying quantum bath effects on quantum transfer mechanisms. *J. Chem. Phys.* **2012**, *136*, 224103.
(57) Weiss, U. *Quantum Dissipative Systems*; World Scientific, 2011; p 588.
(58) Feynman, R. P.; Vernon, F. L. The theory of a general quantum system interacting with a linear dissipative system. *Ann. Phys. (Amsterdam, Neth.)* **1963**, *24*, 118.
(59) Moyal, J. E.; Bartlett, M. S. Quantum mechanics as a statistical theory. *Math. Proc. Cambridge Philos. Soc.* **1949**, *45*, 99.
(60) İmre, K.; Özizmir, E.; Rosenbaum, M.; Zweifel, P. F. Wigner Method in Quantum Statistical Mechanics. *J. Math. Phys.* **1967**, *8*, 1097.
(61) Tanaka, M.; Tanimura, Y. Quantum Dissipative Dynamics of Electron Transfer Reaction System: Nonperturbative Hierarchy Equations Approach. *J. Phys. Soc. Jpn.* **2009**, *78*, 073802.
(62) Davies, R. W. The Connection between the Smoluchowski Equation and the Kramers-Chandrasekhar Equation. *Phys. Rev.* **1954**, *93*, 1169−1170.
(63) Risken, H. *The Fokker−Planck Equation*; Springer-Verlag: Berlin, 1989; Vol. *18*.
(64) Ankerhold, J. *Quantum Tunneling in Complex Systems: The Semiclassical Approach*; Springer-Verlag: Berlin, 2007.
(65) Ankerhold, J.; Grabert, H. Erratum: Strong Friction Limit in Quantum Mechanics: The Quantum Smoluchowski Equation [Phys. Rev. Lett. 87, 086802 (2001)]. *Phys. Rev. Lett.* **2008**, *101*, 119903.
(66) Maier, S. A.; Ankerhold, J. Quantum Smoluchowski equation: A systematic study. *Phys. Rev. E* **2010**, *81*, 021107.
(67) Maier, S. A.; Ankerhold, J. Low-temperature quantum fluctuations in overdamped ratchets. *Phys. Rev. E* **2010**, *82*, 021104.
(68) Roy, S.; Bagchi, B. Time dependent solution of generalized Zusman model of outersphere electron transfer reactions: Applications to various experimental situations. *J. Chem. Phys.* **1994**, *100*, 8802.
(69) Zusman, L. D.; Beratan, D. N. Two-electron transfer reactions in polar solvents. *J. Chem. Phys.* **1996**, *105*, 165−176.
(70) Ankerhold, J.; Lehle, H. Low temperature electron transfer in strongly condensed phase. *J. Chem. Phys.* **2004**, *120*, 1436−1449.
(71) Zhu, L.; Liu, H.; Shi, Q. A new method to account for the difference between classical and quantum baths in quantum dissipative dynamics. *New J. Phys.* **2013**, *15*, 095020.
(72) Härtle, R.; Cohen, G.; Reichman, D. R.; Millis, A. J. Decoherence and lead-induced interdot coupling in nonequilibrium electron transport through interacting quantum dots: A hierarchical quantum master equation approach. *Phys. Rev. B: Condens. Matter Mater. Phys.* **2013**, *88*, 235426.
(73) Härtle, R.; Cohen, G.; Reichman, D. R.; Millis, A. J. Transport through an Anderson impurity: Current ringing, nonlinear magnetization, and a direct comparison of continuous-time quantum Monte Carlo and hierarchical quantum master equations. *Phys. Rev. B: Condens. Matter Mater. Phys.* **2015**, *92*, 085430.
(74) Yan, Y.-a. Low-Storage Runge-Kutta Method for Simulating Time-Dependent Quantum Dynamics. *Chin. J. Chem. Phys.* **2017**, *30*, 277.
(75) Frensley, W. R. Wigner-function model of a resonant-tunneling semiconductor device. *Phys. Rev. B: Condens. Matter Mater. Phys.* **1987**, *36*, 1570.
(76) Frensley, W. R. Boundary conditions for open quantum systems driven far from equilibrium. *Rev. Mod. Phys.* **1990**, *62*, 745.
(77) Kim, K.-Y. A discrete formulation of the Wigner transport equation. *J. Appl. Phys.* **2007**, *102*, 113705.
(78) Tanimura, Y. Reduced hierarchical equations of motion in real and imaginary time: Correlated initial states and thermodynamic quantities. *J. Chem. Phys.* **2014**, *141*, 044114.
(79) Tanimura, Y.; Mukamel, S. Real-time path-integral approach to quantum coherence and dephasing in nonadiabatic transitions and nonlinear optical response. *Phys. Rev. E: Stat. Phys., Plasmas, Fluids, Relat. Interdiscip. Top.* **1993**, *47*, 118−136.
(80) Stock, G.; Thoss, M. Classical Description of Nonadiabatic Quantum Dynamics. *Adv. Chem. Phys.* **2005**, *131*, 243−375.
(81) May, V.; Kühn, O. *Charge and Energy Transfer Dynamics in Molecular Systems*; John Wiley & Sons, 2008.
(82) Hammes-Schiffer, S.; Tully, J. C. Proton transfer in solution: Molecular dynamics with quantum transitions. *J. Chem. Phys.* **1994**, *101*, 4657.
(83) Tuckerman, M. *Statistical Mechanics: Theory and Molecular Simulation*; Oxford University Press, 2010.
(84) Torii, H. Effects of Intermolecular Vibrational Coupling and Liquid Dynamics on the Polarized Raman and Two-Dimensional Infrared Spectral Profiles of Liquid N,N-Dimethylformamide Analyzed with a Time-Domain Computational Method. *J. Phys. Chem. A* **2006**, *110*, 4822−4832.
(85) Jansen, T. l. C.; Knoester, J. Nonadiabatic Effects in the Two-Dimensional Infrared Spectra of Peptides: Application to Alanine Dipeptide. *J. Phys. Chem. B* **2006**, *110*, 22910−22916.
(86) Tempelaar, R.; van der Vegte, C. P.; Knoester, J.; Jansen, T. L. C. Surface hopping modeling of two-dimensional spectra. *J. Chem. Phys.* **2013**, *138*, 164106.
(87) Ferrario, M.; Grigolini, P. The non-Markovian relaxation process as a "contraction" of a multidimensional one of Markovian type. *J. Math. Phys.* **1979**, *20*, 2567−2572.
(88) Marchesoni, F.; Grigolini, P. On the extension of the Kramers theory of chemical relaxation to the case of nonwhite noise. *J. Chem. Phys.* **1983**, *78*, 6287−6298.
(89) Senitzky, I. R. Dissipation in Quantum Mechanics. The Harmonic Oscillator. *Phys. Rev.* **1960**, *119*, 670−679.
(90) Schmid, A. On a quasiclassical Langevin equation. *J. Low Temp. Phys.* **1982**, *49*, 609−626.
(91) Martens, C. C. Qualitative dynamics of generalized Langevin equations and the theory of chemical reaction rates. *J. Chem. Phys.* **2002**, *116*, 2516−2528.
(92) Kawai, S. On the environmental modes for the generalized Langevin equation. *J. Chem. Phys.* **2015**, *143*, 094101.

DOI: 10.1021/acs.jctc.8b01195
J. Chem. Theory Comput. 2019, 15, 2517−2534